# Engineering arbitrary motional ionic states through realistic intensity-fluctuating laser pulses

R. M. Serra,[1,*] P. B. Ramos,[1] N. G. de Almeida,[1] W. D. José,[2] and M. H. Y. Moussa[1,†]
[1]*Departamento de Física, Universidade Federal de São Carlos, P.O. Box 676, São Carlos, 13565-905, Sao Paulo, Brazil*
[2]*Departamento de Ciências Exatas e Tecnológicas, Universidade Estadual de Santa Cruz, Rodovia Ilhéus-Itabuna, km 16, Ilhéus, 45650-000, Bahia, Brazil*

(Received 3 October 2000; published 19 April 2001)

We present a reliable scheme for engineering arbitrary motional ionic states through an adaptation of the projection synthesis technique for trapped-ion phenomena. Starting from a prepared coherent motional state, the Wigner function of the desired state is thus sculpted from a Gaussian distribution. The engineering process has also been developed to take into account the errors arising from intensity fluctuations in the exciting-laser pulses required for manipulating the electronic and vibrational states of the trapped ion. To this end, a recently developed phenomenological-operator approach that allows for the influence of noise will be applied. This approach furnishes a straightforward technique to estimate the fidelity of the prepared state in the presence of errors, precluding the usual extensive *ab initio* calculations. The results obtained here by the phenomenological approach, to account for the effects of noise in our engineering scheme, can be directly applied to any other process involving trapped-ion phenomena.

DOI: 10.1103/PhysRevA.63.053813 PACS number(s): 42.50.Vk, 42.50.Ct, 32.90.+a, 03.65.Ta

## I. INTRODUCTION

In recent years, experimental advances in the domain of cavity quantum electrodynamics (QED) and trapped ions have motivated increasing interest in the engineering of nonclassical states. The preparation of quantum states constitutes a crucial step towards testing fundamentals of quantum mechanics, such as nonlocality and decoherence [1], and to the development of devices such as logic gates for implementing quantum computation [2]. Theoretical schemes have been put forward for engineering arbitrary states of the radiation field, both trapped in high-$Q$ cavities [3–6] and as a traveling wave [7,8], besides electronic and vibrational states of trapped ions [9–13].

In Refs. [3–5], the desired superposition of photon-number state in a cavity field is engineered from the vacuum state, photon by photon. In the scheme of Vogel *et al.* [3], resonant atom-field interactions are required to create a general single-mode resonator, while Parkins *et al.* [4] suggest a method using adiabatic transfer of Zeeman coherence, and Law and Eberly [5] have provided an approach without the need to prepare multilevel electronic superpositions. In Ref. [6] the authors, despite starting from a coherent state of the cavity field, do not provide a scheme for generating an arbitrary superposition state. In the traveling-wave domain, Barnett and Pegg [7] proposed a method to generate an arbitrary superposition of a zero- and one-photon field state, based on state truncation of traveling optical fields. A similar scheme for generating arbitrary quantum states of a traveling wave was proposed by Dakna *et al.* [8].

Concerning the engineering of trapped-ionic states, a technique for preparing even and odd coherent motional states of a trapped ion, via laser excitation of two vibrational transition, has been described by de Matos Filho and Vogel [9]. Starting from the vacuum state as in Ref. [9], Kneer and Law [10] proposed a scheme for generating a general quantum entanglement of the electronic and vibrational states of a trapped ion, besides discussing the engineering of two vibrational degrees of freedom of a single-trapped ion. Brobný *et al.* [11] also provide a technique for deterministic preparation of two-mode vibrational states. A method for creating deterministic electronic Bell states of two-trapped ions was reported by Solano *et al.* [12] , and Moya-Cessa *et al.* [13] presented a procedure to generate arbitrary discrete superpositions of vibrational coherent states.

The preparation of a variety of nonclassical states has been achieved in cavity QED [1,14,16] and trapped-ion phenomena [17,18]. ''Schrödinger cat''-like states of both the radiation field trapped in superconducting cavities [1] and quantized-motional states of trapped ions [17] have been achieved experimentally. The preparation of pure photon number states of the radiation field has been recently reported [16].

The feasibility of engineering trapped-ionic states relies on the fact that decoherence of quantum superpositions can be made negligible by suppressing spontaneous emission using metastable transitions. Coherence of the atomic population survives for many Rabi cycles of the Jaynes-Cummings (JC) interaction [15], during which, at sufficiently low pressure, collisions with background atoms can also be avoided [19]. Here we mention a recent, remarkable experimental achievement in which the decoherence of superposed motional states of a single-trapped ion was controlled through engineered-quantum reservoirs [20]. To accomplish this, laser-cooling techniques have been considered to generate an effectively zero-temperature reservoir as suggested in Ref. [21]. Different from processes in cavity QED, where the cavity-damping mechanism is the source of errors and decoherence, in the domain of trapped ions it is assumed that the errors arise from fluctuating-electrical fields of the trap and intensity and phase fluctuations in the exciting laser pulses [22]. Stochastic models have been proposed to deal with

*Electronic address: serra@df.ufscar.br
†Electronic address: miled@power.ufscar.br

 

these sources of errors [23–26], and they are shown to be in good qualitative agreement with recent experiments. Recently, instead of a stochastic mechanism, Di Fidio and Vogel [27] proposed a model where the observed damping in Rabi oscillations [19] is caused by quantum jumps to an auxiliary electronic level. Other less important error sources in trapped ions, such as collisions with the background gas, are also present [23,28].

An advantage of engineering trapped-ionic states over cavity-field states is that the latter is a more demanding process. In fact, a bunch of two-level atoms are required to generate a cavity field, each atom being appropriately prepared by a Ramsey zone (in a particular superposition state), with its velocity selected before interacting with the cavity field, and detected before the passage of the subsequent atom [29]. On the other hand, the preparation of an ionic state is designed by just switching laser pulses on and off, alternately, to manipulate the electronic and vibrational states of the trapped ion. However, we show here that the errors introduced by the intensity fluctuation in the exciting laser pulses has a severe effect on the engineered state, even more dramatic than the errors introduced by the cavity-damping mechanism when preparing a cavity-field state [31].

In this paper we present a scheme for engineering an arbitrary motional state of a trapped ion by the *projection synthesis* method, which was originally proposed in the traveling-wave domain [7] for the measurement of particular properties of the radiation field, such as its phase [32] or its $Q$ function [33]. This scheme consists of sculpting an arbitrary motional ionic state from a coherent motional state previously prepared in the ionic trap. The technique of sculpting an arbitrary state from a coherent superposition through the projection-synthesis technique was previously developed in the cavity QED domain [29]. However, here we take advantage of the facility to manipulate trapped ions to make this process even more attractive in terms of experimental implementation. In the cavity QED domain, the sculpture technique [29] considerably improves previous schemes for generating an arbitrary state of the radiation field [3]. Whereas in Ref. [3] $N$ atoms are required to generate a field with a maximum number of photons equal to $N$, this technique requires about half of this number, exactly $M=\mathrm{int}[(N+1)/2]$. This is due to the fact that we begin our process from a coherent state previously injected into the cavity, instead of the vacuum state as in [3]. So, instead of building up the desired state photon by photon, we proceed to sculpt an existing coherent state with an appropriate average excitation previously calculated. The situation is analogous to the present proposal for creating motional ionic states. Instead of requiring $N$ steps to generate an arbitrary motional state with a maximum number of phonons equal to $N$ [10], our technique utilizes just $M$ steps, as in the cavity QED context.

We stress that in the present work we elaborate the engineering process of the vibrational ionic state in the realistic presence of noise. Following the reasoning in Ref. [23], we consider the noise arising from the intensity fluctuations of the laser pulses used to manipulate the electronic and vibrational states of the trapped ion. Thus, after discussing the fundamental interactions between the trapped ion and a classical field in Sec. II, we describe our technique for preparing the ionic-vibrational state in the ideal case (absence of noise) in Sec. III. In Sec. IV, we calculate the fidelity of a sculpted state under the effects of noise. Here, a phenomenological-operator approach [30,31] will be applied to account for the presence of noise in the engineering process. This approach has been developed precisely to compute the effects of noise in complex processes such as quantum state engineering and teleportation of quantum states; processes where the protocol requires several steps of quantum interactions. Through the phenomenological-operator approach, first developed in the domain of cavity QED [30,31], the effect of noise is introduced directly in the evolution of the state vector of the whole system, instead of turning to the evolution of the density operator as in the *ab initio* methods. In Sec. V we present a technique for optimizing the fidelity of the sculpted state that is based on an appropriate choice of the ion-laser interaction parameters in the expression of the sculpted state computed in the presence of noise. Also in Sec. V, we illustrate the scheme by sculpting a phase state and computing the *fidelity-probability rate*, a cost-benefit estimate for sculpting a desired state, as defined in Sec. III. Finally, in Sec. VI we give a summary and draw conclusions.

## II. MODEL

We consider one single-trapped ion of mass $m$ in a one-dimensional harmonic trap whose frequency is $\nu$. The ion has forbidden transitions between two internal electronic states (excited $|\uparrow\rangle$ and ground $|\downarrow\rangle$ states, taken as hyperfine sublevels of the ground state), separated by frequency $\omega_0$ and indirectly coupled by interactions with two laser beams, of frequencies $\omega_1$ and $\omega_2$ , in a stimulated Raman-type configuration. As indicated in Fig. 1, the laser beams are detuned by $\Delta$ from a third more excited level $|r\rangle$ that, in the stimulated Raman-type configuration, is adiabatically eliminated when $\Delta$ is much larger than all of the following: the linewidth of level $|r\rangle$, the coupling associated with the $|\uparrow\rangle\leftrightarrow|r\rangle$ and $|\downarrow\rangle\leftrightarrow|r\rangle$ transitions, and the detuning $\delta\equiv\omega_0-\omega_L$ $(\omega_L=\omega_1-\omega_2)$ [34,35]. The transition between $|\downarrow\rangle$ and a fourth level $|d\rangle$, achieved by another laser strongly coupled to the electronic ground state, is considered in order to measure the ionic-vibrational state by collecting the resonance fluorescence signal, which is the probability of the ion being found in the internal state $|\downarrow\rangle$ [18].

The Hamiltonian that describes the effective interaction of the quantized motion of the ionic center of mass (c.m.) with its electronic degree of freedom is [18,34] in a frame rotating at the ''effective laser frequency'' $\omega_L$ $(\hbar=1)$,

$$\hat{H}=\nu\hat{a}^{\dagger}\hat{a}+\frac{\delta}{2}\hat{\sigma}_z+\Omega(\hat{\sigma}_- e^{-i\eta(\hat{a}+\hat{a}^{\dagger})+i\varphi}+\hat{\sigma}_+ e^{i\eta(\hat{a}+\hat{a}^{\dagger})-i\varphi}), \tag{1}$$

where $\varphi$ is the phase difference between the two lasers, $\hat{\sigma}_+=|\uparrow\rangle\langle\downarrow|$, $\hat{\sigma}_-=|\downarrow\rangle\langle\uparrow|$ and $\hat{\sigma}_z$ are the usual Pauli pseudospin

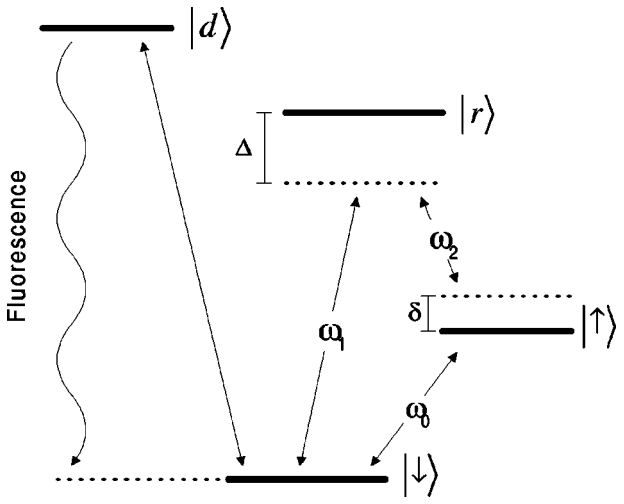


FIG. 1. Electronic energy level diagram of a trapped ion interacting with the laser beams of frequency $\omega_1$ and $\omega_2$, where $\delta=\omega_1-\omega_2-\omega_0$ ($\delta \ll \Delta$), $|r\rangle$ (adiabatically eliminated) is an auxiliary electronic level that indirectly couples the levels $|\uparrow\rangle$ and $|\downarrow\rangle$, and $|d\rangle$ is an electronic level used to measure the fluorescence emission.

operators, $\hat{a}^\dagger$ ($\hat{a}$) is the creation (annihilation) operator of vibrational quanta, $\Omega$ is the effective Rabi frequency of the transition $|\uparrow\rangle \leftrightarrow |\downarrow\rangle$ and, $\eta$ is the Lamb-Dicke parameter defined as [18,35]

$$\eta=\frac{\Delta k}{\sqrt{2m\nu}}. \tag{2}$$

Here $\Delta k=(\vec{k}_1-\vec{k}_2)\cdot\vec{i}, |\vec{k}_{1(2)}|=\omega_{1(2)}/c$, $\vec{k}_1$ ($\vec{k}_2$) being the wave vector for laser 1 (2), and $\vec{i}$ is the unit vector in the direction of the trap axis .

Written $H$ in the interaction picture and then expanding the resulting Hamiltonian in terms of the Lamb-Dicke parameter we get

$$\hat{H}_I=\Omega e^{-\eta^2/2}\left[\sum_{m,l=0}^{\infty}\frac{(i\eta)^{m+l}}{m!l!}\times\exp\{-i[(m-l)\nu+\delta]t+i\varphi\}\hat{a}^{\dagger m}\hat{a}^l\hat{\sigma}_- + \text{H.c.}\right]. \tag{3}$$

Assuming the Lamb-Dicke limit, for which $\eta \ll 1$, where the ionic c.m. motion is strongly localized with respect to the laser wavelengths, we obtain the simplified Hamiltonian

$$\hat{H}_I=\Omega(e^{-i\delta t+i\varphi}\hat{\sigma}_- + i\eta e^{-i(\nu+\delta)t+i\varphi}\hat{a}^\dagger\hat{\sigma}_- + i\eta e^{-i(-\nu+\delta)t+i\varphi}\hat{a}\hat{\sigma}_- + \text{H.c.}),$$

where resonance is achieved by tuning the laser frequencies to obtain $\delta=-\ell\nu$ ($\ell=m-l$). Considering the realistic value for the trap frequency $\nu/2\pi\approx 11.2$ MHz [15], the optical rotating wave approximation leads to the carrier Hamiltonian ($\ell=0$) when tuning the effective laser frequency to obtain $\delta=0$,

$$\hat{H}_c=\Omega(\hat{\sigma}_+ e^{-i\varphi}+\hat{\sigma}_- e^{i\varphi}). \tag{4}$$

This Hamiltonian induces the transition $|n,\downarrow\rangle \leftrightarrow |n,\uparrow\rangle$ (where $|n\rangle$ indicates a motional Fock state), and is responsible for rotating only the internal electronic levels of the ion wave function in accordance with

$$e^{-i\hat{H}_c\tau}|n,\uparrow\rangle=\cos(\Omega\tau)|n,\uparrow\rangle - ie^{i\varphi}\sin(\Omega\tau)|n,\downarrow\rangle, \tag{5a}$$

$$e^{-i\hat{H}_c\tau}|n,\downarrow\rangle=\cos(\Omega\tau)|n,\downarrow\rangle - ie^{-i\varphi}\sin(\Omega\tau)|n,\uparrow\rangle. \tag{5b}$$

When tuning the effective laser frequency to obtain $\delta=-\nu$, the optical rotating wave approximation leads to the Jaynes-Cummings like Hamiltonian ($\ell=1$) corresponding to the first red sideband,

$$\hat{H}_{JC}=i\Omega\eta(\hat{a}\hat{\sigma}_+ e^{-i\varphi}-\hat{a}^\dagger\hat{\sigma}_- e^{i\varphi}), \tag{6}$$

which induces the transition $|n,\downarrow\rangle \leftrightarrow |n-1,\uparrow\rangle$, in such a way that the electronic and vibrational modes evolve as

$$e^{-i\hat{H}_{JC}\tau}|n,\uparrow\rangle=C_n|n,\uparrow\rangle - e^{-i\varphi}S_n|n+1,\downarrow\rangle, \tag{7a}$$

$$e^{-i\hat{H}_{JC}\tau}|n,\downarrow\rangle=C_{n-1}|n,\downarrow\rangle + e^{i\varphi}S_{n-1}|n-1,\uparrow\rangle, \tag{7b}$$

where $C_n=\cos(g\tau\sqrt{n+1})$, $S_n=\sin(g\tau\sqrt{n+1})$, $\tau$ is the duration of the laser pulses, and $g=\Omega\eta$. Finally, we note that it is possible to obtain the anti-Jaynes-Cummings Hamiltonian ($\ell=-1$) corresponding to the first blue sideband. However, for the purposes of the present paper we do not use this specific interaction that induces the transition $|n,\downarrow\rangle \leftrightarrow |n+1,\uparrow\rangle$.

## III. SCULPTURE SCHEME (IDEAL CASE)

In this section we show how to transpose the *projection-synthesis* technique from its original traveling-wave domain [7] to the context of the ionic trap (similar to Ref. [29] where the *projection synthesis* was applied to cavity QED phenomena). We assume the trapped ion to be initially prepared with its c.m. in a coherent motional state $|\alpha\rangle$, and in the electronic excited state $|\uparrow\rangle$. Such a state, which can be prepared with techniques available nowadays [17,18], reads

$$|\Psi^{(0)}\rangle=|\alpha\rangle\otimes|\uparrow\rangle=\sum_{n=0}^{\infty}\Lambda_n^{(0)}|n\rangle\otimes|\uparrow\rangle, \tag{8}$$

with $\Lambda_n^{(0)}=\exp(-|\alpha|^2/2)\alpha^n/\sqrt{n!}$. As the desired state is generated from a previous coherent state, we have denominated the present scheme a quantum state sculpture process (as originally done in [29]). In fact, as shown below, our strategy consists of modeling the Wigner function of the desired state, through appropriate laser pulses, from that of the previously prepared motional coherent state in Eq. (8). The car-

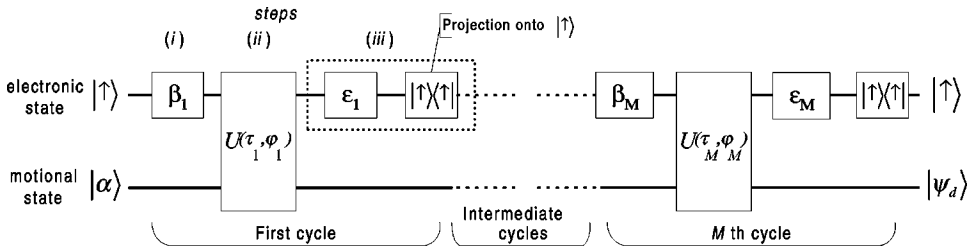


FIG. 2. A quantum-algorithm notation [36] for the process of sculpting arbitrary motional states. The complex parameters $\beta_k$ and $\varepsilon_k$ indicate rotations of the electronic states by the first and second $C$ pulses, respectively, in the $k$th cycle and are adjusted by an appropriate choice of the duration and phase of the laser field following Eqs. (5a,b). $U(\tau_k,\varphi_k)$ indicates the evolution operator for the $k$th JC pulse. At the end of each cycle the measurement of absence of fluorescence (projection on to $|\uparrow\rangle$) is required for the successful accomplishment of the engineering process. The time proceeds from left to right, as usual.

rier ($C$) and the JC laser pulses work as ''quantum chisels'' on the initial coherent distribution, as shown in the quantum-algorithm notation [36] depicted in Fig. 2. In the domain of cavity QED, the quantum chisels are represented by two-level Rydberg atoms that are made to interact resonantly with a coherent state initially prepared in a high-$Q$ cavity [29].

The whole operation is accomplished in three-step cycles, requiring successively: (i) a carrier pulse $C_1$, to prepare the electronic state in a suitable superposition, (ii) a first red sideband pulse JC, to entangle the ionic motional and electronic states, and, finally, (iii) a sequence of a carrier pulse $C_2$ and a fluorescence measurement of the ionic electronic state. The third step constitutes the projection synthesis, which enables us to synthesize the measurement of a particular superposition of the electronic state and, consequently, to synthesize the projection of the motional degree of freedom to the desired sculpted state. Thus, the projection-synthesis technique is here applied to both of the entangled degrees of freedom of the trapped ion, electronic, and motional (analogously, in the cavity QED domain we synthesized the simultaneous projection of the atomic and the cavity-field states [29]). A fluorescent signal projects the ion into state $|\downarrow\rangle$, while the absence of fluorescence projects it into state $|\uparrow\rangle$. For the present purpose the absence of fluorescence is crucial in preventing the occurrence of recoil of the ionic c.m. motion. So, at the end of each cycle the detection of the absence of fluorescence is required for the successful accomplishment of the engineering process. We emphasize that the duration of the fluorescence measurement is an order of magnitude smaller than that of the JC pulse and about half that of a $C$ pulse in experiments involving the usual parameter values [15]. For a JC pulse, $g\tau=\pi/2$ and for a $C$ pulse, $\Omega\tau=\pi/2$, the respective durations being around 2 $\mu$s and 0.5 $\mu$s, while the time for a fluorescence signal is around 0.2 $\mu$s [37]. We repeat this three-step cycle $M$ times to synthesize an arbitrary desired state $|\Psi_d\rangle=\Sigma_{n=0}^{N_d} d_n|n\rangle\otimes|\uparrow\rangle$ (see Fig. 2), where it should be noted that the electronic state $|\uparrow\rangle$ factorizes. The parameters $M$ and $N_d$ (the maximal excitation number of the desired state) are related as shown below.

Considering the $k$th cycle of the sculpture process, let us start with the assumption that the ionic state after the $(k-1)$th cycle is

$$|\Psi^{(k-1)}\rangle=\sum_{n=0}^{\infty}\Lambda_n^{(k-1)}|n,\uparrow\rangle. \tag{9}$$

As the first step of the $k$th cycle we prepare, with the carrier pulse $C_1$, the electronic state in the superposition $\mathcal{N}_{\beta_k}(|\uparrow\rangle+\beta_k|\downarrow\rangle)$, where $\mathcal{N}_{\beta_k}=(1+|\beta_k|^2)^{-1/2}$ and $\beta_k$ is a complex parameter adjusted by pulse $C_1$, fixed at an appropriate duration and phase of the carrier pulse [as in Eqs. (5a) and (5b)]. In the second step, the first red sideband pulse JC entangles the ionic motional and electronic states as

$$|\psi^{(k)}\rangle=\mathcal{N}_{\beta_k}\sum_{n=0}^{\infty}\Lambda_n^{(k-1)}(C_n^{(k)}|n,\uparrow\rangle-e^{-i\varphi_k}S_n^{(k)}|n+1,\downarrow\rangle+\beta_k C_{n-1}^{(k)}|n,\downarrow\rangle+e^{i\varphi_k}\beta_k S_{n-1}^{(k)}|n-1,\uparrow\rangle), \tag{10}$$

where $C_m^{(k)}=\cos(g\tau_k\sqrt{m+1})$, $S_m^{(k)}=\sin(g\tau_k\sqrt{m+1})$, $\tau_k$ and $\varphi_k$ are the $k$th JC pulse duration and phase, respectively. Next, in the third step, we have to synthesize the projection of state (10) into a particular electronic superposition state (of the $k$th cycle) $|\chi^{(k)}\rangle=\mathcal{N}_{\varepsilon_k}(|\uparrow\rangle+\varepsilon_k^*|\downarrow\rangle)$, with $\mathcal{N}_{\varepsilon_k}=(1+|\varepsilon_k|^2)^{-1/2}$. The complex number $\varepsilon_k$ results from the $k$th rotation of the electronic states induced by the second carrier pulse $C_2$. As a consequence of the absence of fluorescent signal (which is the case of a successful measurement), the ionic state after the projection synthesis is given by

$$|\Psi^{(k)}\rangle=\mathcal{N}_k|\uparrow\rangle\langle\chi^{(k)}|\psi^{(k)}\rangle=\sum_{n=0}^{\infty}\Lambda_n^{(k)}|n,\uparrow\rangle. \tag{11}$$

The coefficients $\Lambda_n^{(k)}$ result from those in Eq. (10) using the recurrence formula $\Lambda_n^{(k)}=\mathcal{N}_k\Gamma_n^{(k)}$, where

$$\Gamma_n^{(k)}=(C_n^{(k)}+\varepsilon_k\beta_k C_{n-1}^{(k)})\Lambda_n^{(k-1)}+e^{i\varphi_k}\beta_k S_n^{(k)}\Lambda_{n+1}^{(k-1)}-e^{-i\varphi_k}\varepsilon_k(1-\delta_{n,0})S_{n-1}^{(k)}\Lambda_{n-1}^{(k-1)}, \tag{12}$$

and the normalization constant $\mathcal{N}_k$ is given by

$$\mathcal{N}_k=\left[\sum_{n=0}^{\infty}\left|\Gamma_n^{(k)}\right|^2\right]^{-1/2}. \tag{13}$$

The pulse $C_2$ and the absence of fluorescence signal (detecting the state $|\uparrow\rangle$) are needed in order to adjust the measurement of the special superposition $|\chi^{(k)}\rangle$, during which they play the role of electronic state ''polarizers'' and ''analyz

ers,'' respectively—by analogy with light-polarization measurement—and allow us to analyze an arbitrary superposition of $|\uparrow\rangle$ and $|\downarrow\rangle$. Such a measurement [38] works as follows: The carrier pulse $C_2$ is appropriately adjusted so that the electronic state of the ion in the superposition $|\chi^{(k)}\rangle$ undergoes a unitary transformation to the state $|\uparrow\rangle$. Otherwise, the electronic state evolves to $|\downarrow\rangle$ if it was initially orthogonal to $|\chi^{(k)}\rangle$. After the carrier pulse $C_2$ a fluorescence measurement is required to project $|\uparrow\rangle$ or $|\downarrow\rangle$. In general, the electronic state after the JC pulse will be a superposition of these orthogonal states, so that in unsuccessful cases we find a fluorescence signal (detecting $|\downarrow\rangle$), and in successful cases we do not (detecting $|\uparrow\rangle$). Once we find the absence of fluorescence the electronic state in the $k$th cycle has been projected on the required superposition $|\chi^{(k)}\rangle$. Thus, the projection synthesis technique is able to measure observables of the form $|\chi^{(k)}\rangle\langle\chi^{(k)}|$, which represent projection operators with measurable eigenvalues associated with absence (detecting $|\uparrow\rangle$) or presence (detecting $|\downarrow\rangle$) of a fluorescent signal.

Here we stress an important difference between the present sculpture process and that used to prepare an arbitrary state in cavity QED [29]. In the latter, the projection synthesis is achieved by measuring the required two-level Rydberg atoms (the quantum chisels for sculpting the field state), each in a particular superposition state, through a classical field and ionization chamber detectors. Hence, after the projection synthesis, the measured state of the $k$th atom is discarded, since it turns to be useless for the cavity QED process, whereas the electronic state of the ion, factored as $|\uparrow\rangle$ in a successful event, is ready for the next cycle. Therefore, the motional state of the ion is sculpted by means of its own electronic states.

Since the projection of a particular electronic state in the $M$th cycle is supposed to finish the sculpture process, the following equality must be satisfied:

$$\mathcal{N}_M|\uparrow\rangle\langle\chi^{(M)}|\psi^{(M)}\rangle=\sum_{n=0}^{\infty}\Lambda_n^{(M)}|n,\uparrow\rangle=\sum_{n=0}^{N_d}d_n|n,\uparrow\rangle, \tag{14}$$

requiring that $\Lambda_n^M\approx 0$ when $n\geqslant N_d+1$. This approximation results in a nonunity *fidelity* for the sculpted state. Usually, the fidelity of a given quantum process is defined to account for the inevitable errors introduced by the environment due to dissipative mechanisms [30,31]. However, as mentioned in the Introduction, in the domain of trapped ions it is assumed that the errors arise from noise due to fluctuations in the trap and laser parameters [22], and to treat this error source we consider the stochastic model proposed in [23], where just the intensity fluctuations of the laser pulses are considered. In this section we focus on the ideal case in which the fidelity is defined to account only for the errors introduced by the approximation ($\Lambda_n^M\approx 0$ for $n\geqslant N_d+1$) inherent in this sculpture scheme. So, this fidelity, which does not account for the errors introduced by the environment or fluctuations, reads

$$\mathcal{F}\equiv|\langle\Psi_d|\psi^{(M)}\rangle|^2=\frac{\left|\sum_{n=0}^{N_d}d_n^*\Gamma_n^{(M)}\right|^2}{\sum_{l=0}^{\infty}|\Gamma_l^{(M)}|^2}. \tag{15}$$

The total probability of successfully sculpting the desired state is $\mathcal{P}=\Pi_{k=1}^{M}P_k$, where $P_k$ is the probability of synthesizing a particular electronic superposition, $|\langle\chi^{(k)}|\psi^{(k)}\rangle|^2$, from the $k$th entanglement between motional and electronic states, Eq. (10). In other words, $P_k$ refers to the probability of measuring absence of fluorescence after the second carrier pulse in the $k$th cycle. This probability is given by

$$P_k=|\langle\chi^{(k)}|\psi^{(k)}\rangle|^2=\mathcal{N}_{\varepsilon_k}^2\mathcal{N}_{\beta_k}^2\sum_{n=0}^{\infty}|\Gamma_n^k|^2. \tag{16}$$

For an appropriate choice of average excitation of the coherent motional state, $|\alpha|^2=\overline{n}_\alpha$, we see from the recurrence formula (12) and the definition of coefficients $\Lambda_n^{(0)}$, that the coefficients $\Gamma_n^{(M)}$ depend on powers of $\alpha$, varying as $\alpha^j/\sqrt{j!}$, with $n-M\leqslant j\leqslant n+M$. In fact, it is straightforward to conclude that, after one application of formula (12) the coefficients $\Gamma_n^{(M)}$ are proportional to $\{\Lambda_{n-1}^{(M-1)},\Lambda_n^{(M-1)},\Lambda_{n+1}^{(M-1)}\}$; after two applications of the formula it follows that

$$\Gamma_n^{(M)}\propto\{\Lambda_{n-2}^{(M-2)},\Lambda_{n-1}^{(M-2)},\Lambda_n^{(M-2)},\Lambda_{n+1}^{(M-2)},\Lambda_{n+2}^{(M-2)}\}$$

and after $M$ applications we finally obtain

$$\Gamma_n^{(M)}\propto\{\Lambda_{n-M}^{(0)},\Lambda_{n-M+1}^{(0)},\ldots,\Lambda_n^{(0)},\ldots,\Lambda_{n+M-1}^{(0)},\Lambda_{n+M}^{(0)}\}.$$

.

Therefore, from the definition of $\Lambda_n^{(0)}$ (initial coherent motional state), we note that $\Gamma_n^{(M)}$ depends on powers of $\alpha$, as mentioned above, and the choice of the average excitation $\overline{n}_\alpha$ that ensures $P(N_d-M+1)=|\langle N_d-M+1|\alpha\rangle|^2\approx 0$ (satisfying the requirement that $\Lambda_n^{(M)}\approx 0$ when $n\geqslant N_d+1$) results in a higher fidelity $\mathcal{F}$ at the expense of a lower probability $\mathcal{P}$. In fact, it is evident from the denominator of Eq. (15) that lower the number $l$ in the sum of significant coefficients, the higher the fidelity. On the other hand, in Eq. (16) we observe that the probability $\mathcal{P}$ is directly proportional to powers of $\alpha$. As a consequence, Eqs. (15) and (16) furnish a fidelity-probability rate, $\mathcal{R}\equiv\mathcal{F}^{\xi},\mathcal{P}^{\zeta}$, a cost-benefit estimate for sculpting the desired state, where the parameters $\xi$ and $\zeta$ are appropriately chosen to weight the contributions of the fidelity and the probability in accordance with the aims of the sculptor. In fact, the sculptor may decide to privilege the fidelity or the probability in the cost-benefit estimative, and in the present work we have decided to privilege the fidelity, choosing the values $\xi=4$ and $\zeta=1/2$. In order to maximize the rate $\mathcal{R}$, we have to play with all the parameters: the durations and phases of the JC laser pulses, $\tau_k$ and $\varphi_k$, and the carrier pulse ($C_1$ and $C_2$) parameters $\beta_k$ and $\varepsilon_k$. We note that a good strategy to maximize $\mathcal{R}$ consists in starting

with a choice of $\bar{n}_\alpha$ so that $P(N_d-M+1)\approx 0$, and then proceed to maximize the rate $\mathcal{R}$, increasing $\bar{n}_\alpha$ at the expense of the fidelity. Next, the duration and phase of the JC laser pulses $\tau_k$ and $\varphi_k$ are chosen so as to maximize the rate $\mathcal{R}$. Finally, the choice of the carrier pulse parameters, $\beta_k$ and $\varepsilon_k$, follows from a particular solution of the equality (14) that, together with the requirement $\Lambda_n^{(M)}\approx 0$ when $n \geqslant N_d+1$, results in the set of $N_d+1$ equations

$$
\begin{aligned}
d_{N_d} &= \mathcal{N}_M[(C_{N_d}^{(M)}+\varepsilon_M\beta_M C_{N_d-1}^{(M)})\Lambda_{N_d}^{(M-1)} \\
&\quad + e^{i\varphi_k}\beta_M S_{N_d}^{(M)}\Lambda_{N_d+1}^{(M-1)} - e^{-i\varphi_k}\varepsilon_M S_{N_d-1}^{(M)}\Lambda_{N_d-1}^{(M-1)}], \\
&\vdots \\
d_n &= \mathcal{N}_M[(C_n^{(M)}+\varepsilon_M\beta_M C_{n-1}^{(M)})\Lambda_n^{(M-1)} + e^{i\varphi_k}\beta_M S_n^{(M)}\Lambda_{n+1}^{(M-1)} \\
&\quad - e^{-i\varphi_k}\varepsilon_M S_{n-1}^{(M)}\Lambda_{n-1}^{(M-1)}], \qquad (17) \\
&\vdots \\
d_0 &= \mathcal{N}_M[(C_0^{(M)}+\varepsilon_M\beta_M)\Lambda_0^{(M-1)} + e^{i\varphi_k}\beta_M S_0^{(M)}\Lambda_1^{(M-1)}].
\end{aligned}
$$

To solve the set of Eqs. (17), we apply the recurrence formula (12) $M-1$ times in order to express the unknown coefficients $\Lambda_n^{(k)}$ in terms of the known values of the coefficients of the coherent motional state, $\Lambda_n^{(0)}$. In this way we obtain a nonlinear system whose free parameters are $\beta_1,\ldots,\beta_M$ and $\varepsilon_1,\ldots,\varepsilon_M$, which indicate the particular rotation the electronic state must undergo in each cycle, during each carrier pulse ($C_1$ and $C_2$). These variables are obtained from the known coefficients $d_n$ and $\Lambda_n^{(0)}$. The solvability of a nonlinear system can be ensured if the number of equations is equal to the number of variables, the latter being the parameters of both carrier pulses. One of the equations in system (17) has to be used to obtain the normalization constant $\Pi_{k=1}^{M}\mathcal{N}_k$ and each cycle carries two free parameters $(\beta_k,\varepsilon_k)$. Therefore, the minimum number of cycles necessary to guarantee the solution of system (17) must be $M=\mathrm{int}\,[(N_d+1)/2]$. This conclusion follows from the fact that in our scheme we start from a coherent motional state. The real variables $\tau_1,\tau_2,\ldots,\tau_M$ and $\phi_1,\phi_2\ldots\phi_M$ are used to improve the cost-benefit rate $R$.

With this technique, therefore, it is possible to sculpt an arbitrary vibrational state by remodeling another initial vibrational state. In particular, we have started from the coherent state since it is easily generated [18].

### A. Sculpting a truncated phase state

To illustrate the sculpture technique we now proceed to engineer the truncated-phase state ($N_d=2$)

$$
|\Psi_d\rangle = \frac{1}{\sqrt{3}}\sum_{n=0}^{2}|n,\uparrow\rangle. \qquad (18)
$$

As mentioned above, the sculpture process for the state $|\Psi_d\rangle$ requires just $M=1$ cycle, and we obtain from Eqs. (17) the system

$$
\frac{[(C_2^{(1)}+\varepsilon_1\beta_1 C_1^{(1)})\Lambda_2^{(0)} + e^{i\varphi_1}\beta_1 S_2^{(1)}\Lambda_3^{(0)} - e^{-i\varphi_1}\varepsilon_1 S_1^{(0)}\Lambda_1^{(0)}]}{[(C_0^{(1)}+\varepsilon_1\beta_1)\Lambda_0^{(0)} + e^{i\varphi_1}\beta_1 S_0^{(1)}\Lambda_1^{(0)}]} = 1, \qquad (19a)
$$

$$
\frac{[(C_1^{(M)}+\varepsilon_1\beta_1 C_0^{(1)})\Lambda_1^{(0)} + e^{i\phi_1}\beta_1 S_1^{(1)}\Lambda_2^{(0)} - e^{-i\phi_1}\varepsilon_1 S_0^{(1)}\Lambda_0^{(0)}]}{[(C_0^{(1)}+\varepsilon_1\beta_1)\Lambda_0^{(0)} + e^{i\varphi_1}\beta_1 S_0^{(1)}\Lambda_1^{(0)}]} = 1. \qquad (19b)
$$

Solving the above system we obtain a fourth-order polynomial equation in the variable $\varepsilon_1$ ($\beta_1$) by isolating the variable $\beta_1$ ($\varepsilon_1$) from one equation and substituting it into the other. In this way we obtain the roots of the system (19a) and (19b) for any fixed set of parameters $\bar{n}_\alpha$, $g\tau_1$ and $\varphi_1$. When considering more than one cycle to sculpt a state where $N_d>2$, instead of Eqs. (19a) and (19b) we obtain a set of $N_d$ coupled equations, permitting only numerical solutions ([29]).

Following the strategy mentioned above, we start with the average excitation $\bar{n}_\alpha$ leading to the highest fidelity resulting from $P(3)=|\langle 2|\alpha\rangle|^2\approx 0$. For our purposes we begin with the average excitation $\bar{n}_\alpha=0.04$. For each value of $\bar{n}_\alpha$ (choosing $\alpha$ as a real parameter) we proceed to calculate the duration ($g\tau_1$) and phase ($\varphi_1$) of the JC laser pulse that maximize the rate $\mathcal{R}$. As discussed above, the maximum value of $\mathcal{R}$ depends on the choice of the parameters $\xi=4$ and $\zeta=1/2$, weighting $\mathcal{F}$ and $\mathcal{P}$, respectively. In Table I we show the rate $\mathcal{R}$ associated with each value of $\bar{n}_\alpha$, from that which maximizes the fidelity (0.04) to values that exhibit a continuous decrease of the rate $\mathcal{R}$. In addition, four roots $(\varepsilon_1,\beta_1)$ of Eqs. (19a) and (19b) result when a given pair of parameters $(g\tau_1,\varphi_1)$ are fixed, and we have to choose the one that maximizes $\mathcal{R}$. The value $\bar{n}_\alpha=0.25$ results in the highest rate $\mathcal{R}=0.60$, which follows from a fidelity $\mathcal{F}=0.99$ and probability $\mathcal{P}=0.38$ of successfully sculpting the desired state.

We display in Figs. 3(a) and 3(b) the sculpture process of the desired truncated phase state (18) from the Wigner-distribution function of the initial coherent state (associated to $\bar{n}_\alpha=0.25$) given by a Gaussian shifted from the origin as

TABLE I. The probability $\mathcal{P}$, fidelity $\mathcal{F}$, and rate $\mathcal{R}=\mathcal{F}^{\xi}\mathcal{P}^{\zeta}$ (with $\xi=4$ and $\zeta=1/2$), for each value of averaged-excitation number $\bar{n}_{\alpha}$. The JC pulse interaction time $g\tau_1$ and phase $\varphi_1$ in this table correspond to values that maximize the rate $\mathcal{R}$ for each $\bar{n}_{\alpha}$.

| $\bar{n}_{\alpha}$ | $g\tau_1$ | $\varphi_1$ | $\mathcal{P}$ | $\mathcal{F}$ | $\mathcal{R}$ |
|---|---|---|---|---|---|
| 0.04 | 3.35 | 3.15 | 0.11 | 0.99 | 0.33 |
| 0.09 | 3.51 | 3.14 | 0.22 | 0.99 | 0.47 |
| 0.16 | 3.65 | 3.15 | 0.33 | 0.99 | 0.56 |
| 0.25 | 3.79 | 3.14 | 0.38 | 0.99 | 0.60 |
| 0.36 | 3.93 | 3.14 | 0.42 | 0.97 | 0.59 |
| 0.49 | 4.07 | 0.02 | 0.44 | 0.95 | 0.53 |
| 0.64 | 1.81 | 3.14 | 0.61 | 0.92 | 0.54 |

$W(p,q)=(2/\pi)\exp[-(q+\alpha)^2-p^2]$, shown in Fig. 3(a). The state (associated with the best rate $\mathcal{R}=0.60$) obtained after one cycle is displayed in Fig. 3(b), using the parameters ($g\tau_1,\varphi_1,\varepsilon_1$ and $\beta_1$) associated with this rate. As we have stressed above, it is possible by the present scheme to sculpt the desired state with a higher probability of sucess but at the expense of a smaller fidelity. So, the sculpture technique can be evaluated by a cost-benefit estimate, here defined as the fidelity-probability rate, which is up to the sculptor to choose.

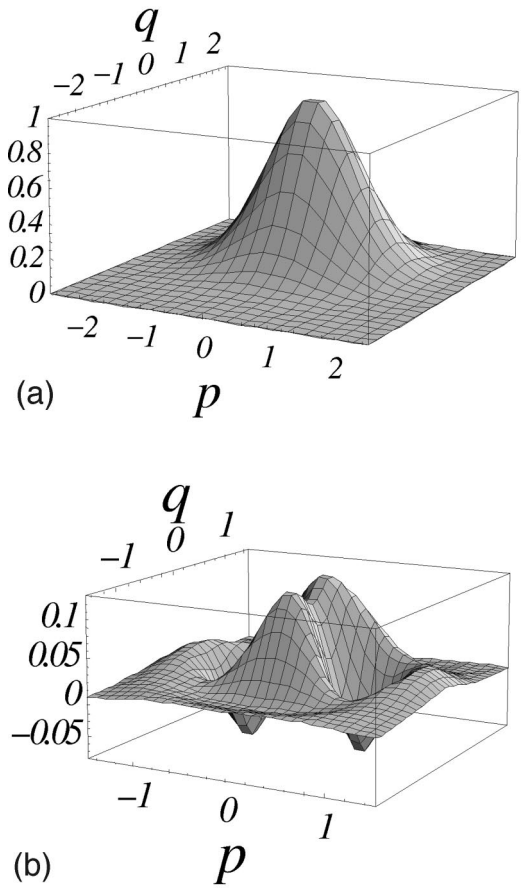


FIG. 3. Wigner-distribution functions for (a) the initial coherent state associated with $\bar{n}_{\alpha}=0.25$ and for (b) the modified state after the first cycle. We have used the values $\varepsilon_1=25.615\,9-0.0379I$ and $\beta_1=-0.399\,4-0.640\,8I\times10^{-4}$ associated with the values in Table I: $\mathcal{F}=0.99$, $\mathcal{P}=0.38$, and $\mathcal{R}=0.60$.

The next section deals with the effects of noise on the sculpture process, i.e., the influence of the errors arising from the intensity fluctuations in the exciting laser pulses. In this paper we do not consider either the (weaker) effects of the phase fluctuations of the laser pulses [23] or the (close to unity) efficiency of detection of the internal state required in the third step of the cycle [22]. When the effects of noise on the sculpture process are taken into account, following the phenomenological-operator approach, the fidelity defined by Eq. (15) remains exactly the same, whereas the sculpt field state, after the last-required cycle, will be entangled with auxiliary states in which noise operators are defined. So, to the best of our knowledge the sculpted motional state will be represented by a statistical mixture $\rho_{ion}$, whereby the fidelity turns out to be $\mathcal{F}=\langle\psi_d|\rho_{ion}|\psi_d\rangle$.

## IV. EFFECTS OF NOISE ON THE PROCESS

As mentioned above, we consider here the noise arising from the intensity fluctuations in the exciting laser pulses (carrier and Jaynes-Cummings) required to manipulate the internal and external states of the trapped ion [23,28]. We will also propose an alternative way of engineering an ionic motional state in the presence of noise, which consists in maximizing the fidelity of the experimentally achieved state. A phenomenological-operator approach, originally developed in the context of cavity QED [30,31], will be considered here to account for the evolution of the ionic states under the influence of the fluctuating-intensity laser pulses. The strategy is to provide a straightforward technique to incorporate the main results obtained by standard *ab initio* methods for treating errors in trapped ions (in particular we consider the master-equation calculations in Ref. [23]). In short, we introduce an auxiliary state space where noise operators are defined to allow for the effects of noise explicitly in the evolution of the state vector of the whole system comprehended by the ionic and auxiliary states. After computing the evolved state of the whole system, the reduced-density matrix of the ionic system can immediately be obtained by tracing out the auxiliary variables. The phenomenological approach is constructed so that the reduced-density matrix turns out to be exactly the same as the one obtained by standard methods. It is interesting to note that the phenomenological approach resembles the Monte Carlo wave function method [39] in the sense that we work directly with the wave function, providing an efficient computational tool.

First we give a short description of the master-equation treatment by Schneider and Milburn [23] of the laser fluctuations as a stochastic process, the rise or fall of the laser intensity being defined as a real Wiener process. After the pulses required to generate the desired state, the noise introduced is effectively averaged and the master equation describing the ionic system follows from the stochastic Liouville–von Neumann equation [23]

$$\frac{d}{dt}\hat{\rho}(t) = -i[\hat{\mathcal{H}},\hat{\rho}(t)] - \frac{\Gamma}{2}[\hat{\mathcal{H}},[\hat{\mathcal{H}},\hat{\rho}(t)]] \tag{20}$$

where $\hat{\mathcal{H}}$ is the interaction Hamiltonian for the $C$ (4) or JC (6) pulse and the parameter $\Gamma$, to be obtained phenomenologically, scales the noise. Considering the subspace composed of the eigenstates of $\hat{\mathcal{H}}$, it is straightforward to solve Eq. (20), obtaining

$$\langle \Phi_n^{\pm}|\rho(t)|\Phi_m^{\pm}\rangle = \exp[-it(\Phi_n^{\pm}-\Phi_m^{\pm}) - 2\Gamma t(\Phi_n^{\pm}-\Phi_m^{\pm})^2] \times \langle \Phi_n^{\pm}|\rho(0)|\Phi_m^{\pm}\rangle \tag{21}$$

where $|\Phi_m^{\pm}\rangle$ are the eigenstates and $\Phi_n^{\pm}$ are the eigenvalues for the interaction Hamiltonian described by Eqs. (4) and (6). For the $C$ Hamiltonian,

$$|\Phi_n^{\pm}\rangle = \frac{1}{\sqrt{2}}(|n\downarrow\rangle \pm e^{i\varphi}|n\uparrow\rangle),$$

$$\Phi_n^{\pm} = \pm\Omega,$$

while for the JC Hamiltonian,

$$|\Phi_n^{\pm}\rangle = \frac{1}{\sqrt{2}}(|n,\downarrow\rangle \pm ie^{i\phi}|n-1,\uparrow\rangle),$$

$$\Phi_n^{\pm} = \pm g\sqrt{n}.$$

Employing the reasoning of the phenomenological-operator approach, we have introduced the noise operators $\hat{\mathcal{C}}$ and $\hat{\mathcal{J}}$, to account for the intensity fluctuations in the $C$ and the JC pulses, respectively. These operators are supposed to act on the auxiliary states $|\mathbf{C}\rangle$ and $|\mathbf{J}\rangle$, so as to the effects of noise explicitly in the evolution of the whole system, now composed of the ionic and auxiliary states. After the ion-laser interactions required for the sculpture process, the reduced-density operator of the ion is obtained by tracing out the auxiliary space describing the noise sources.

With the noise operators defined in the auxiliary spaces, we observe that the coupling of a general ionic state to the fluctuating $C$ laser pulses evolves in time as,

$$\sum_n (\alpha_n|n\downarrow\rangle + \beta_n|n\uparrow\rangle)\otimes|\mathbf{C}\rangle \rightarrow |\Psi_C\rangle$$

$$= \sum_n [\alpha_n\hat{\mathcal{C}}_{n,\downarrow\downarrow}(t,\varphi) + \beta_n\hat{\mathcal{C}}_{n,\uparrow\downarrow}(t,\varphi)]|n\downarrow\rangle\otimes|\mathbf{C}\rangle + [\alpha_n\hat{\mathcal{C}}_{n,\downarrow\uparrow}(t,\varphi) + \beta_n\hat{\mathcal{C}}_{n,\uparrow\uparrow}(t,\varphi)]|n\uparrow\rangle\otimes|\mathbf{C}\rangle \tag{22}$$

while for the JC pulse it follows

$$\sum_n (\alpha_n|n,\downarrow\rangle + \beta_n|n,\uparrow\rangle)\otimes|\mathbf{J}\rangle \rightarrow |\Psi_{JC}\rangle$$

$$= \sum_n [\alpha_n\hat{\mathcal{J}}_{n,\downarrow\downarrow}(t,\varphi)|n,\downarrow\rangle + \beta_n\hat{\mathcal{J}}_{n,\uparrow\downarrow}(t,\varphi)|n+1,\downarrow\rangle + \alpha_n\hat{\mathcal{J}}_{n\downarrow\uparrow}(t,\varphi)|n-1,\uparrow\rangle + \beta_n\hat{\mathcal{J}}_{n,\uparrow\uparrow}(t,\varphi)|n,\uparrow\rangle]\otimes|\mathbf{J}\rangle. \tag{23}$$

Following the reasoning of the phenomenological approach, the matrix elements $\langle\mathbf{C}|\hat{\mathcal{C}}_{n,jk}(t,\varphi)\hat{\mathcal{C}}^{\dagger}_{n|j|k|}(t,\varphi)|\mathbf{C}\rangle$ and $\langle\mathbf{J}|\hat{\mathcal{J}}_{n,jk}(t,\varphi)\hat{\mathcal{J}}^{\dagger}_{n|,j|k|}(t,\varphi)|\mathbf{J}\rangle$ $(n,n^{|}=0,1,2\ldots,\ j,\ j^{|}=\uparrow,\downarrow$ and $k,k^{|}=\uparrow,\downarrow)$, which result from tracing the density operator associated with Eqs. (22) and (23) over the auxiliary spaces $\mathbf{C}$ and $\mathbf{J}$ ($\mathrm{Tr}_{\mathbf{C(JC)}}\ |\Psi_{C(JC)}\rangle\langle\Psi_{C(JC)}| = \rho^{red}_{C(JC)}$), are inferred from the standard-stochastic method in [23]. Comparing the reduced-density operator $\rho^{red}_{C(JC)}$ with those emerging from the evolution in Eq. (21) of the density matrix associated with the state $\Sigma_n(\alpha_n|n\downarrow\rangle + \beta_n|n\uparrow\rangle)$, we obtain the required matrix elements shown in Appendix A. Such matrix elements can now be directly applied to any process that involves interactions of an ion with fluctuating-intensity laser pulses, removing the necessity to perform the typically extensive *ab initio* calculations. In the case of a process requiring several laser pulses (as when sculpting a state with a large $N_d$) it turns to be practically prohibitive to compute the evolution of the ionic system by standard techniques.

### A. Estimating the errors introduced by $C$ and JC pulses

Let us now consider the initial state $|\psi_C(0)\rangle = |\psi_{JC}(0)\rangle = |n,\downarrow\rangle$, which evolves, in the ideal case (without fluctuations), following Eqs. (5b) and (7b) for carrier and Jaynes-Cummings pulses, respectively:

$$|\psi_C(t)\rangle = e^{-i\hat{H}_c\tau}|\psi_c(0)\rangle = \cos(\Omega t)|n,\downarrow\rangle - ie^{-i\varphi}\sin(\Omega t)|n,\uparrow\rangle,$$

$$|\psi_{JC}(t)\rangle = e^{-i\hat{H}_{JC}\tau}|\psi_{JC}(0)\rangle = \cos(gt\sqrt{n})|n,\downarrow\rangle + e^{i\varphi}\sin(gt\sqrt{n})|n-1,\uparrow\rangle,$$

where $t$ and $\varphi$ are the duration and phase for both pulses. Now, given realistic intensity fluctuations in the laser pulses, the evolution of states $|\psi_c(0)\rangle$ and $|\psi_{JC}(0)\rangle$ is easily computed with the phenomenological approach, leading to the results

$$|\tilde{\psi}_C(t)\rangle\otimes|\mathbf{C}\rangle = [\hat{\mathcal{C}}_{n,\downarrow\downarrow}(t,\varphi)|n,\downarrow\rangle + \hat{\mathcal{C}}_{n,\downarrow\uparrow}(t,\varphi)|n,\uparrow\rangle]\otimes|\mathbf{C}\rangle,$$

$$|\tilde{\psi}_{JC}(t)\rangle\otimes|\mathbf{J}\rangle = [\hat{\mathcal{J}}_{n,\downarrow\downarrow}(t,\varphi)|n,\downarrow\rangle + \hat{\mathcal{J}}_{n,\downarrow\uparrow}(t,\varphi)|n-1,\uparrow\rangle]\otimes|\mathbf{J}\rangle.$$

The reduced-density operator of the ion (obtained by tracing out the auxiliary spaces $\mathbf{C}$ and $\mathbf{J}$) are

$$\begin{aligned}\hat{\tilde{\rho}}_C(t) &= \mathrm{Tr}_{\mathbf{C}}|\tilde{\psi}_C(t)\rangle|\mathbf{C}\rangle\langle\mathbf{C}|\langle\tilde{\psi}_C(t)| \\ &= \langle\hat{\mathcal{C}}_{n,\downarrow\downarrow}(t,\varphi)\hat{\mathcal{C}}^{\dagger}_{n,\downarrow\downarrow}(t,\varphi)\rangle_{\mathbf{C}}|n,\downarrow\rangle\langle n,\downarrow| \\ &\quad + \langle\hat{\mathcal{C}}_{n,\downarrow\downarrow}(t,\varphi)\hat{\mathcal{C}}^{\dagger}_{n,\downarrow\uparrow}(t,\varphi)\rangle_{\mathbf{C}}|n,\downarrow\rangle\langle n,\uparrow| \\ &\quad + \langle\hat{\mathcal{C}}_{n,\downarrow\uparrow}(t,\varphi)\hat{\mathcal{C}}^{\dagger}_{n,\downarrow\downarrow}(t,\varphi)\rangle_{\mathbf{C}}|n,\uparrow\rangle\langle n,\downarrow| \\ &\quad + \langle\hat{\mathcal{C}}_{n,\downarrow\uparrow}(t,\varphi)\hat{\mathcal{C}}^{\dagger}_{n,\downarrow\uparrow}(t,\varphi)\rangle_{\mathbf{C}}|n,\uparrow\rangle\langle n,\uparrow|,\end{aligned}$$

$$\begin{aligned}\hat{\tilde{\rho}}_{JC}(t) &= \mathrm{Tr}_{\mathbf{J}}|\tilde{\psi}_{JC}(t)\rangle|\mathbf{J}\rangle\langle\mathbf{J}|\langle\tilde{\psi}_c(t)| \\ &= \langle\hat{\mathcal{J}}_{n,\downarrow\downarrow}(t,\varphi)\hat{\mathcal{J}}^{\dagger}_{n,\downarrow\downarrow}(t,\varphi)\rangle_{\mathbf{J}}|n,\downarrow\rangle\langle n,\downarrow| \\ &\quad + \langle\hat{\mathcal{J}}_{n,\downarrow\downarrow}(t,\varphi)\hat{\mathcal{J}}^{\dagger}_{n,\downarrow\uparrow}(t,\varphi)\rangle_{\mathbf{J}}|n,\downarrow\rangle\langle n-1,\uparrow| \\ &\quad + \langle\hat{\mathcal{J}}_{n,\downarrow\uparrow}(t,\varphi)\hat{\mathcal{J}}^{\dagger}_{n,\downarrow\downarrow}(t,\varphi)\rangle_{\mathbf{J}}|n-1,\uparrow\rangle\langle n,\downarrow| \\ &\quad + \langle\hat{\mathcal{J}}_{n,\downarrow\uparrow}(t,\varphi)\hat{\mathcal{J}}^{\dagger}_{n,\downarrow\uparrow}(t,\varphi)\rangle_{\mathbf{J}}|n-1,\uparrow\rangle\langle n-1,\uparrow|.\end{aligned}$$

From the matrix elements shown in Appendix A and after a straightforward calculation we obtain the following fidelities of the evolved states $|\tilde{\psi}_C(t)\rangle$ and $|\tilde{\psi}_{JC}(t)\rangle$ with respect to the ideal evolution of $|\psi_C(0)\rangle$ and $|\psi_{JC}(0)\rangle$

$$\mathcal{F}_C = \langle\psi_C(t)|\hat{\rho}_c(t)|\psi_C(t)\rangle = \frac{1}{2} + \frac{1}{2}e^{-2\Gamma\Omega^2 t},$$

$$\mathcal{F}_{JC} = \langle\psi_{JC}(t)|\hat{\rho}_{JC}(t)|\psi_{JC}(t)\rangle = \frac{1}{2} + \frac{1}{2}e^{-2n\Gamma g^2 t},$$

for carrier and Jaynes-Cummings pulses, respectively. Note that for $\Gamma=0$ we have $\mathcal{F}_c=\mathcal{F}_{JC}=1$, as expected. Besides, for $n=0$ we have $\mathcal{F}_{JC}=1$ since the intensity fluctuations in the JC pulse do not exchange energy with the ionic system, maintaining the initial state $|n=0,\downarrow\rangle$ unaffected. As defined in Sec. II, $g=\eta\Omega$, and the Lamb-Dicke parameter used in experiments is $\eta=0.202$ [15]; thus, the noise introduced by the JC pulse has less effect than that coming from the $C$ pulse for $n \lesssim 25$. Thus, when sculpting the phase state (18) or in any process involving a small number of phonons, such as engineering a motional qubit state $c_0|0\rangle+c_1|1\rangle$ for quantum computation, as performed in [40], the main source of errors will undoubtedly be the $C$ pulses.

### B. Sculpting a truncated phase state in the presence of noise

Now we proceed to incorporate the intensity fluctuations of the laser pulses used in sculpting the truncated-phase state (18) that is obtained after one cycle of the sculpture process. We assume, for simplicity, that there is no noise in the preparation of the initial coherent motional state of the ion. After the preparation of such a motional state and the first- carrier pulse it follows that

$$\begin{aligned}\sum_{n=0}^{\infty}\Lambda_n^{(0)}|n,\uparrow\rangle\otimes|\mathbf{C}_1\rangle \rightarrow \sum_{n=0}^{\infty}\Lambda_n^{(0)}[\hat{\mathcal{C}}_{n,\uparrow\downarrow}(t_1)|n\downarrow\rangle \\ + \hat{\mathcal{C}}_{n,\uparrow\uparrow}(t_1)|n\uparrow\rangle]\otimes|\mathbf{C}_1\rangle = |\psi^I\rangle,\end{aligned}$$

where $t_1$ is the duration of the first-carrier pulse and $\mathbf{C}_1$ stands for its auxiliary space. To simplify the notation we have omitted that the operator $\hat{\mathcal{C}}$ depends on the phase $\varphi_1$ of the $C$ laser pulse. Note that in this first step the required superposition of the electronic state $\mathcal{N}_\beta(|\uparrow\rangle+\beta_k|\downarrow\rangle)$ is obtained with a nonunity fidelity due to laser fluctuations. In the second step, the first red sideband pulse JC entangles the ionic motional and electronic states as

$$\begin{aligned}|\psi^I\rangle\otimes|\mathbf{J}\rangle \rightarrow \sum_{n=0}^{\infty}\Lambda_n^{(0)}[\hat{\mathcal{J}}_{n\downarrow\downarrow}(t_2)\hat{\mathcal{C}}_{n\uparrow\downarrow}(t_1)|n,\downarrow\rangle \\ + \hat{\mathcal{J}}_{n\uparrow\downarrow}(t_2)\hat{\mathcal{C}}_{n\uparrow\uparrow}(t_1)|n+1,\downarrow\rangle \\ + \hat{\mathcal{J}}_{n\downarrow\uparrow}(t_2)\hat{\mathcal{C}}_{n\uparrow\downarrow}(t_1)|n-1,\uparrow\rangle \\ + \hat{\mathcal{J}}_{n\uparrow\uparrow}(t_2)\hat{\mathcal{C}}_{n\uparrow\uparrow}(t_1)|n,\uparrow\rangle]\otimes|\mathbf{J},\mathbf{C}_1\rangle = |\psi^{II}\rangle,\end{aligned}$$

where $t_2$ and $\varphi_2$ are the duration and phase of the JC laser pulse. Finally, after the second $C$ pulse we have

$$\begin{aligned}|\psi^{II}\rangle\otimes|\mathbf{C}_2\rangle \rightarrow \sum_{n=0}^{\infty}\Lambda_n^{(0)}[\{\hat{\mathcal{C}}_{n,\downarrow\downarrow}(t_3)\hat{\mathcal{J}}_{n,\downarrow\downarrow}(t_2)\hat{\mathcal{C}}_{n,\uparrow\downarrow}(t_1,\varphi_1) \\ + \hat{\mathcal{C}}_{n,\uparrow\downarrow}(t_3)\hat{\mathcal{J}}_{n,\uparrow\uparrow}(t_2)\hat{\mathcal{C}}_{n,\uparrow\uparrow}(t_1)\}|n,\downarrow\rangle \\ + \hat{\mathcal{C}}_{n+1,\downarrow\downarrow}(t_3)\hat{\mathcal{J}}_{n\uparrow\downarrow}(t_2)\hat{\mathcal{C}}_{n,\uparrow\uparrow}(t_1)|n+1,\downarrow\rangle \\ + \hat{\mathcal{C}}_{n+1,\downarrow\uparrow}(t_3)\hat{\mathcal{J}}_{n\uparrow\downarrow}(t_2)\hat{\mathcal{C}}_{n,\uparrow\uparrow}(t_1)|n+1,\uparrow\rangle \\ + \hat{\mathcal{C}}_{n-1,\uparrow\uparrow}(t_3)\hat{\mathcal{J}}_{n\downarrow\uparrow}(t_2)\hat{\mathcal{C}}_{n,\uparrow\downarrow}(t_1)|n-1,\uparrow\rangle \\ + \hat{\mathcal{C}}_{n-1,\uparrow\downarrow}(t_3)\hat{\mathcal{J}}_{n\downarrow\uparrow}(t_2)\hat{\mathcal{C}}_{n,\uparrow\downarrow}(t_1)|n-1,\downarrow\rangle \\ + \{\hat{\mathcal{C}}_{n,\downarrow\uparrow}(t_3)\hat{\mathcal{J}}_{n,\downarrow\downarrow}(t_2)\hat{\mathcal{C}}_{n,\uparrow\downarrow}(t_1) \\ + \hat{\mathcal{C}}_{n,\uparrow\uparrow}(t_3)\hat{\mathcal{J}}_{n,\uparrow\uparrow}(t_2)\hat{\mathcal{C}}_{n,\uparrow\uparrow}(t_1)\}|n,\uparrow\rangle] \\ \otimes|\mathbf{C}_2,\mathbf{J},\mathbf{C}_1\rangle = |\psi^{III}\rangle.\end{aligned}$$

with $t_3$ and $\varphi_3$ standing for the duration and phase of the second $C$ laser pulse. In the absence of fluorescence signal, the above entangled state $|\psi^{III}\rangle$ evolves to

$$\begin{aligned}|\psi^{IV}\rangle = \mathsf{N}\sum_{n=0}^{\infty}[\Lambda_{n-1}^{(0)}\hat{\mathcal{C}}_{n,\downarrow\uparrow}(t_3)\hat{\mathcal{J}}_{n-1,\uparrow\downarrow}(t_2)\hat{\mathcal{C}}_{n-1,\uparrow\uparrow}(t_1) \\ \times(1-\delta_{n,0}) + \Lambda_{n+1}^{(0)}\hat{\mathcal{C}}_{n,\uparrow\uparrow}(t_3)\hat{\mathcal{J}}_{n+1\downarrow\uparrow}(t_2)\hat{\mathcal{C}}_{n+1,\uparrow\downarrow}(t_1) \\ + \Lambda_n^{(0)}\hat{\mathcal{C}}_{n,\downarrow\uparrow}(t_3)\hat{\mathcal{J}}_{n,\downarrow\downarrow}(t_2)\hat{\mathcal{C}}_{n,\uparrow\downarrow}(t_1) \\ + \Lambda_n^{(0)}\hat{\mathcal{C}}_{n,\uparrow\uparrow}(t_3)\hat{\mathcal{J}}_{n,\uparrow\uparrow}(t_2)\hat{\mathcal{C}}_{n,\uparrow\uparrow}(t_1)]|n\uparrow\rangle \\ \otimes|\mathbf{C}_2,\mathbf{J},\mathbf{C}_1\rangle, \qquad (24)\end{aligned}$$

and tracing out the auxiliary spaces $\mathbf{C}_2$,$\mathbf{J}$ and $\mathbf{C}_1$, the ionic reduced-density matrix follows

$$\hat{\rho}_{ion}(t_1,t_2,t_3)=\mathrm{Tr}_{\zeta_2,\xi,\zeta_1}|\psi^{IV}\rangle\langle\psi^{IV}| =\mathsf{N}^2\sum_{n,m=0}^{\infty}\rho_{n,m}(t_1,t_2,t_3)|n\uparrow\rangle\langle m\uparrow|, \tag{25}$$

where the coefficients $\rho_{n,m}$ are given in Appendix B and the normalization constant reads $\mathsf{N}=(\Sigma_{n=0}^{\infty}\rho_{n,n}(t_1,t_2,t_3))^{-1/2}$. The probability of detecting absence of fluorescence is $\mathcal{P}=1/\mathsf{N}^2$ and the fidelity of the sculpted mixed state is given by

$$\mathcal{F}=\langle\Psi_d|\hat{\rho}_{ion}(t_1,t_2,t_3)|\Psi_d\rangle. \tag{26}$$

We stress that in the present situation we do not have a system of nonlinear equations as in Eq. (17). However, the best parameters (average excitation of initial coherent state, interaction times, and phases of the pulses) to reach the desired state are determined by numerical maximization of the fidelity expression in Eq. (26), as shown below.

## V. ALGORITHM FOR OPTIMIZING THE FIDELITY OF A SCULPTED STATE

We begin by stressing that there is a crucial difference between the sculpture scheme for the ideal case, described in Sec. III, and for the realistic situation with the effects of noise, described in the previous section. In fact, in the protocol proposed in Sec. III, it is necessary to solve a nonlinear system of equations for $\beta_k$ and $\varepsilon_k$, which arise from the recurrence equations relating the amplitudes $\Lambda_k^{(n)}$. On the other hand, when taking into account the intensity fluctuations in the laser pulses, there is no immediate way to extract useful information from a recurrence relation for the operators $\hat{\mathcal{C}}_{n,jk}(t_1)$, $\hat{\mathcal{J}}_{n,jk}(t_2)$, and $\hat{\mathcal{C}}_{n,jk}(t_3)$ ($n=0,1,2\ldots$, $j=\uparrow,\downarrow$ and $k=\uparrow,\downarrow$) associated with each required cycle. Thus, the first question that arises is how can this problem be overcome? We propose the following solution: consider a specific desired motional state to be sculpted and calculate the fidelity of the sculpted-mixed state (26). The resulting expression for the fidelity is considerably involved and a numerical calculation must be performed to obtain the values $t_i$ and $\varphi_i$ ($i=1,2,3$) that maximize the fidelity-probability rate $\mathcal{R}\equiv\mathcal{F}^{\xi}\mathcal{P}^{\zeta}$. Starting then from the average excitation $\overline{n}_{\alpha}$ that leads to the highest fidelity deduced in the ideal case, we proceed by numerical optimization to find the value of $\overline{n}_{\alpha}$ that maximizes the rate $\mathcal{R}$. Following this procedure, to sculpt the phase state (18) under the effects of noise, we find that $\overline{n}_{\alpha}=0.25$ (coincidently the same value as in the ideal case) results in a highest rate $\mathcal{R}=0.64$, which follows from a fidelity $\mathcal{F}=0.91$ and probability $\mathcal{P}=0.86$ of measuring absence of fluorescence.

Figure 4(a) displays the Wigner-distribution function for the desired state (18), which is to be compared with the Wigner function in Fig. 3(b) for the sculpted state in the ideal case, with fidelity $\mathcal{F}=0.99$. Figure 4(b) displays the mixed state sculpted in the presence of noise using the same parameters $\beta_1$ and $\varepsilon_1$ of Fig. 3(b). By comparing both figures we see that the interference terms leading to negative contributions in Fig. 4(b) have diffused into each other and practically cancel out in Fig. 4(b), which correspond to $\mathcal{F}$

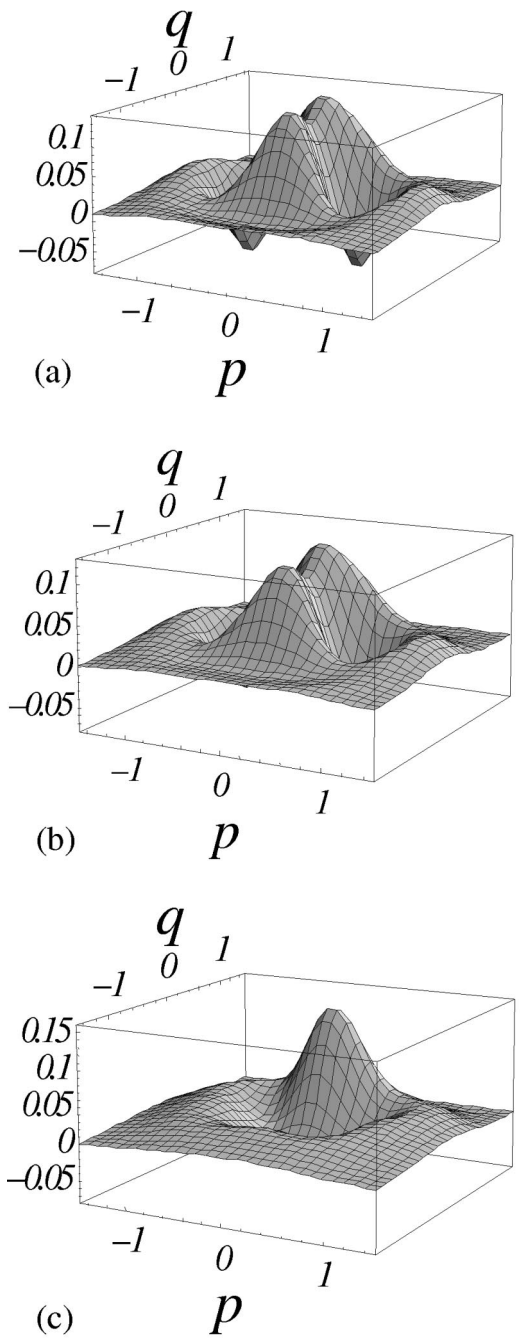


FIG. 4. Wigner-distribution functions for (a) the desired-phase state given in Eq. (18), (b) the mixed state sculpted in the presence of noise using the same parameters $\beta_1$ and $\varepsilon_1$ of Fig. 3(b) ($\mathcal{F}=0.85$ and $\mathcal{P}=0.40$), and (c) the mixed state sculpted through our numerical optimization procedure using the set of parameters $\Omega t_1=0.56$, $\varphi_1=5.48$, $gt_2=0.75$, $\varphi_2=1.40$, $\Omega t_3=1.88$, and $\varphi_3=1.43$ associated with $\mathcal{F}=0.91$, $\mathcal{P}=0.86$, and $\mathcal{R}=0.64$.

$=0.85$ and $\mathcal{P}=0.40$. Finally, Fig. 4(c) displays the mixed state sculpted through our numerical optimization procedure. The fidelity and probability, $\mathcal{F}=0.91$ and $\mathcal{P}=0.86$, respectively, resulting from our optimization procedure are considerably higher than those obtained for the mixed state in Fig. 4(b). It is worth noting that although the Wigner distribution in Fig. 4(b) seems to be closely to the distribution in Fig. 4(a) than that in Fig. 4(c), the optimized-mixed state possesses a higher fidelity, which is just a measure of the distance between the vectors representing the desired and obtained states in Hilbert space and cannot be inferred from the Wigner function (see discussion in Appendix C).

To plot Figs. 4(a)–4(c), we have used realistic values [15] for the Lamb-Dicke parameter, $\eta\simeq 0.202$, Rabi frequency, $\Omega/2\pi\simeq 475$ kHz, and we assume the parameter $\Gamma\approx 10^{-8}$s, estimated in [23] to obtain a good agreement with the experimental results in Ref. [15].

## VI. CONCLUSION

In this work we present a technique to engineer arbitrary ionic motional states employing projection synthesis. This method consists of sculpting the desired motional state from a coherent motional state previously prepared in the ionic trap. The sculpting of arbitrary states from a coherent superposition by projection synthesis was previously developed in the cavity QED domain [29]. However, here we take advantage of the facilities in manipulating trapped ions to make the sculpture process even more attractive for experimental implementation. As in the cavity QED context, instead of requiring $N$ laser pulses to generate an arbitrary motional state with a maximum number of phonons equal to $N$ [10], our technique utilizes just $M=\mathrm{int}[(N+1)/2]$ pulses.

The sculpture scheme was also developed for the realistic situation of intensity fluctuations in the required laser pulses. In this connection, a phenomenological-operator approach developed recently to account for errors in complex quantum processes was applied [30,31]. This approach furnishes a straightforward technique to estimate the fidelity resulting from the engineering process, without the need to perform the usual extended *ab initio* calculations required by standard methods. The reasoning behind the phenomenological approach developed here is to incorporate in a concise algebraic form the main results obtained from the application of the master equation (to the effects of noise arising from the intensity fluctuations in the laser pulses) as done in Ref. [23]. By defining an auxiliary state space where phenomenological operators are defined, we account for the effects of noise explicitly in the evolution of the state vector of the whole system comprehended by the ionic and auxiliary states. After computing the evolved state of the whole system, we can immediately obtain the reduced-density matrix of the ionic system by tracing out the auxiliary variables. We stress that the results obtained here from the phenomenological procedure are quite general, and, in principle, can be applied to any quantum process in an ionic trap, such as quantum communication, logic operations, and teleportation.

As an application of the technique for sculpting an arbitrary motional ionic state, combined with the phenomenological approach to the analysis of the effects of noise in the process, we have computed the fidelity for modifying a truncated-phase state. We assumed realistic values for the parameters involved. Moreover, we have proposed an algorithm to optimize the fidelity of a sculpted state in the presence of noise. This algorithm consists in maximizing the fidelity of the sculpted state (subjected to noise), with regard to the desired state through a convenient choice of the parameters involved in the process. We have also shown, through the phenomenological approach, that the noise introduced by the Jaynes-Cummings pulse has less effect than that coming from the carrier pulse for a number of phonons $n \lesssim 25$. Thus, whether for sculpting a motional state or for any other process involving a small number of phonons, such as engineering a motional qubit state $c_0|0\rangle+c_1|1\rangle$ for quantum computation, as performed in [40], the main source of errors will undoubtedly be the carrier pulses.

## ACKNOWLEDGMENTS

We wish to thank the CNPq and FAPESP, Brazilian agencies.

## APPENDIX A

In this appendix we show explicitly the elements $\langle \mathbf{C}|\hat{\mathcal{C}}_{n,jk}(t,\varphi)\hat{\mathcal{C}}^{\dagger}_{n|j|k|}(t,\varphi)|\mathbf{C}\rangle$ $(n,n^{|}=0,1,2\ldots,\quad j,\quad j^{|}=\uparrow,\downarrow$ and $k,k^{|}=\uparrow,\downarrow)$ for the carrier pulse.

$$\langle \hat{\mathcal{C}}_{n,\downarrow\downarrow}(t,\varphi)\hat{\mathcal{C}}^{\dagger}_{m,\downarrow\downarrow}(t,\varphi)\rangle_{\mathbf{C}}=\langle \hat{\mathcal{C}}_{n,\uparrow\uparrow}(t,\varphi)\hat{\mathcal{C}}^{\dagger}_{m,\uparrow\uparrow}(t,\varphi)\rangle_{\mathbf{C}}$$
$$=\frac{1}{2}[1+\cos(2\Omega t)e^{-2\Gamma\Omega^2 t}],$$

$$\langle \hat{\mathcal{C}}_{n,\uparrow\downarrow}(t,\varphi)\hat{\mathcal{C}}^{\dagger}_{m,\uparrow\downarrow}(t,\varphi)\rangle_{\mathbf{C}}=\langle \hat{\mathcal{C}}_{n,\downarrow\uparrow}(t,\varphi)\hat{\mathcal{C}}^{\dagger}_{m,\downarrow\uparrow}(t,\varphi)\rangle_{\mathbf{C}}$$
$$=\frac{1}{2}[1-\cos(2\Omega t)e^{-2\Gamma\Omega^2 t}],$$

$$\langle \hat{\mathcal{C}}_{n,\downarrow\downarrow}(t,\varphi)\hat{\mathcal{C}}^{\dagger}_{m,\downarrow\uparrow}(t,\varphi)\rangle_{\mathbf{C}}=\langle \hat{\mathcal{C}}_{n,\downarrow\uparrow}(t,\varphi)\hat{\mathcal{C}}^{\dagger}_{m,\downarrow\downarrow}(t,\varphi)\rangle^{*}_{\mathbf{C}}$$
$$=i\frac{e^{-i\varphi}}{2}\sin(2\Omega t)e^{-2\Gamma\Omega^2 t},$$

$$\langle \hat{\mathcal{C}}_{n,\uparrow\uparrow}(t,\varphi)\hat{\mathcal{C}}^{\dagger}_{m,\uparrow\downarrow}(t,\varphi)\rangle_{\mathbf{C}}=\langle \hat{\mathcal{C}}_{n,\uparrow\downarrow}(t,\varphi)\hat{\mathcal{C}}^{\dagger}_{m,\uparrow\uparrow}(t,\varphi)\rangle^{*}_{\mathbf{C}}$$
$$=i\frac{e^{i\varphi}}{2}\sin(2\Omega t)e^{-2\Gamma\Omega^2 t},$$

$$\langle \hat{\mathcal{C}}_{n,\downarrow\downarrow}(t,\varphi)\hat{\mathcal{C}}^{\dagger}_{m,\uparrow\downarrow}(t,\varphi)\rangle_{\mathbf{C}}=\langle \hat{\mathcal{C}}_{n,\uparrow\downarrow}(t,\varphi)\hat{\mathcal{C}}^{\dagger}_{m,\downarrow\downarrow}(t,\varphi)\rangle^{*}_{\mathbf{C}}$$
$$=i\frac{e^{i\varphi}}{2}\sin(2\Omega t)e^{-2\Gamma\Omega^2 t},$$

$$\langle \hat{\mathcal{C}}_{n,\uparrow\downarrow}(t,\varphi)\hat{\mathcal{C}}^{\dagger}_{m,\downarrow\uparrow}(t,\varphi)\rangle_{\mathbf{C}}=\langle \hat{\mathcal{C}}_{n,\downarrow\uparrow}(t,\varphi)\hat{\mathcal{C}}^{\dagger}_{m,\uparrow\downarrow}(t,\varphi)\rangle^{*}_{\mathbf{C}}$$
$$=\frac{e^{-2i\varphi}}{2}[1-\cos(2\Omega t)e^{-2\Gamma\Omega^2 t}],$$

$$\langle \hat{\mathcal{C}}_{n,\downarrow\downarrow}(t,\varphi)\hat{\mathcal{C}}^{\dagger}_{m,\uparrow\uparrow}(t,\varphi)\rangle_{\mathbf{C}} = \langle \hat{\mathcal{C}}_{n,\uparrow\uparrow}(t,\varphi)\hat{\mathcal{C}}^{\dagger}_{m,\downarrow\downarrow}(t,\varphi)\rangle_{\mathbf{C}} = \frac{1}{2}[1+\cos(2\Omega t)e^{-2\Gamma\Omega^2 t}],$$

$$\langle \hat{\mathcal{C}}_{n,\downarrow\uparrow}(t,\varphi)\hat{\mathcal{C}}^{\dagger}_{m,\uparrow\uparrow}(t,\varphi)\rangle_{\mathbf{C}} = \langle \hat{\mathcal{C}}_{n,\uparrow\uparrow}(t,\varphi)\hat{\mathcal{C}}^{\dagger}_{m,\downarrow\uparrow}(t,\varphi)\rangle^{*}_{\mathbf{C}} = -i\frac{e^{i\varphi}}{2}\sin(2\Omega t)e^{-2\Gamma\Omega^2 t}.$$

For the Jaynes Cummings pulse the elements $\langle \mathbf{J}|\hat{\mathcal{J}}_{n,jk}(t,\varphi)\hat{\mathcal{J}}^{\dagger}_{n|,j|k|}(t,\varphi)|\mathbf{J}\rangle$ are

$$\langle \hat{\mathcal{J}}^{\dagger}_{n,\downarrow\downarrow}(t,\varphi)\hat{\mathcal{J}}^{\dagger}_{m,\downarrow\downarrow}(t,\varphi)\rangle_{\mathbf{J}} = \langle \hat{\mathcal{J}}_{n-1,\uparrow\uparrow}(t,\varphi)\hat{\mathcal{J}}^{\dagger}_{m-1,\uparrow\uparrow}(t,\varphi)\rangle_{\mathbf{J}} = \frac{1}{2}[A_{n,m}+B_{n,m}],$$

$$\langle \hat{\mathcal{J}}_{n,\downarrow\downarrow}(t,\varphi)\hat{\mathcal{J}}^{\dagger}_{m-1,\uparrow\downarrow}(t,\varphi)\rangle_{\mathbf{J}} = \langle \hat{\mathcal{J}}_{m,\uparrow\downarrow}(t,\varphi)\hat{\mathcal{J}}^{\dagger}_{n-1,\downarrow\downarrow}(t,\varphi)\rangle^{*}_{\mathbf{J}} = \frac{e^{i\varphi}}{2}[C_{n,m}-D_{n,m}],$$

$$\langle \hat{\mathcal{J}}_{n-1,\uparrow\downarrow}(t,\varphi)\hat{\mathcal{J}}^{\dagger}_{m-1,\uparrow\downarrow}(t,\varphi)\rangle_{\mathbf{J}} = \langle \hat{\mathcal{J}}_{n,\downarrow\uparrow}(t,\varphi)\hat{\mathcal{J}}^{\dagger}_{m,\downarrow\uparrow}(t,\varphi)\rangle_{\mathbf{J}} = \frac{1}{2}[A_{n,m}-B_{n,m}],$$

$$\langle \hat{\mathcal{J}}_{n,\downarrow\downarrow}(t,\varphi)\hat{\mathcal{J}}^{\dagger}_{m+1,\downarrow\uparrow}(t,\varphi)\rangle_{\mathbf{J}} = \langle \hat{\mathcal{J}}_{m,\downarrow\uparrow}(t,\varphi)\hat{\mathcal{J}}^{\dagger}_{n+1,\downarrow\downarrow}(t,\varphi)\rangle^{*}_{\mathbf{J}} = \frac{e^{-i\varphi}}{2}[-C_{n,m+1}+D_{n,m+1}],$$

$$\langle \hat{\mathcal{J}}_{n,\downarrow\downarrow}(t,\varphi)\hat{\mathcal{J}}^{\dagger}_{m,\uparrow\uparrow}(t,\varphi)\rangle_{\mathbf{J}} = \langle \hat{\mathcal{J}}_{m,\uparrow\uparrow}(t,\varphi)\hat{\mathcal{J}}^{\dagger}_{n,\downarrow\downarrow}(t,\varphi)\rangle_{\mathbf{J}} = \frac{1}{2}[A_{n,m+1}+B_{n,m+1}],$$

$$\langle \hat{\mathcal{J}}_{n-1,\uparrow\downarrow}(t,\varphi)\hat{\mathcal{J}}^{\dagger}_{m+1,\downarrow\uparrow}(t,\varphi)\rangle_{\mathbf{J}} = \langle \hat{\mathcal{J}}_{m-1,\downarrow\uparrow}(t,\varphi)\hat{\mathcal{J}}^{\dagger}_{n+1,\uparrow\downarrow}(t,\varphi)\rangle^{*}_{\mathbf{J}} = \frac{e^{-2i\varphi}}{2}[-A_{n,m+1}+B_{n,m+1}],$$

$$\langle \hat{\mathcal{J}}_{n-1,\uparrow\downarrow}(t,\varphi)\hat{\mathcal{J}}^{\dagger}_{m,\uparrow\uparrow}(t,\varphi)\rangle_{\mathbf{J}} = \langle \hat{\mathcal{J}}_{m-1,\uparrow\uparrow}(t,\varphi)\hat{\mathcal{J}}^{\dagger}_{n,\uparrow\downarrow}(t,\varphi)\rangle^{*}_{\mathbf{J}} = -\frac{e^{-i\varphi}}{2}[C_{n,m+1}+D_{n,m+1}],$$

$$\langle \hat{\mathcal{J}}_{n+1,\downarrow\uparrow}(t,\varphi)\hat{\mathcal{J}}^{\dagger}_{m,\uparrow\uparrow}(t,\varphi)\rangle_{\mathbf{J}} = \langle \hat{\mathcal{J}}_{m+1,\uparrow\uparrow}(t,\varphi)\hat{\mathcal{J}}^{\dagger}_{n,\downarrow\uparrow}(t,\varphi)\rangle^{*}_{\mathbf{J}} = -\frac{e^{i\varphi}}{2}[C_{n+1,m+1}+D_{n+1,m+1}],$$

where

$$A_{n,m} = \cos[gt(\sqrt{n}-\sqrt{m})]\exp[-\Gamma g^2 t(\sqrt{n}-\sqrt{m})^2/2],$$

$$B_{n,m} = \cos[gt(\sqrt{n}+\sqrt{m})]\exp[-\Gamma g^2 t(\sqrt{n}+\sqrt{m})^2/2],$$

$$C_{n,m} = \sin[gt(\sqrt{n}-\sqrt{m})]\exp[-\Gamma g^2 t(\sqrt{n}-\sqrt{m})^2/2],$$

and

$$D_{n,m} = \sin[gt(\sqrt{n}+\sqrt{m})]\exp[-\Gamma g^2 t(\sqrt{n}+\sqrt{m})^2/2].$$

## APPENDIX B:

In this appendix we show explicitly the elements $\rho_{n,m}(t_1,t_2,t_3)$,

$$\rho_{n,m}(t_1,t_2,t_3) = \Lambda^{(0)}_{n-1}(\Lambda^{(0)}_{m-1})^{*}\frac{1}{8}[1-\cos(2\Omega t_3)e^{-2\Gamma\Omega^2 t_3}][A_{n,m}(t_2)-B_{n,m}(t_2)][1+\cos(2\Omega t_1)e^{-2\Gamma\Omega^2 t_1}](1-\delta_{n,0})$$

$$\times(1-\delta_{m,0}) + -\Lambda^{(0)}_{n-1}(\Lambda^{(0)}_{m+1})^{*}\frac{e^{i\varphi_3}}{8}$$

$$\times\sin(2\Omega t_3)e^{-2\Gamma\Omega^2 t_3}e^{-2i\varphi_2}[-A_{n,m+1}(t_2)+B_{n,m+1}(t_2)]e^{i\varphi_1}\sin(2\Omega t_1)e^{-2\Gamma\Omega^2 t_1}(1-\delta_{n,0})$$

$$\times + \Lambda^{(0)}_{n-1}(\Lambda^{(0)}_{m})^{*}\frac{i}{8}[1-\cos(2\Omega t_3)e^{-2\Gamma\Omega^2 t_3}]e^{-i\varphi_2}[-C_{n,m}(t_2)-D_{n,m}(t_2)]e^{i\varphi_1}\sin(2\Omega t_1)e^{-2\Gamma\Omega^2 t_1}(1-\delta_{n,0})$$

$$\times + \Lambda^{(0)}_{n-1}(\Lambda^{(0)}_{m})^{*}i\frac{e^{i\varphi_3}}{8}\sin(2\Omega t_3)e^{-2\Gamma\Omega^2 t_3}\times e^{-i\varphi_2}[C_{n,m+1}(t_2)+D_{n,m+1}(t_2)][1+\cos(2\Omega t_1)e^{-2\Gamma\Omega^2 t_1}]$$

$$\times(1-\delta_{n,0})+\Lambda_{n+1}^{(0)}(\Lambda_{m-1}^{(0)})^{*}\frac{e^{-i\varphi_3}}{8}\sin(2\Omega t_3)e^{-2\Gamma\Omega^2 t_3}e^{+2i\varphi_2}[-A_{n+1,m}(t_2)$$

$$+B_{n+1,m}(t_2)]e^{-i\varphi_1}\sin(2\Omega t_1)e^{-2\Gamma\Omega^2 t_1}(1-\delta_{m,0})+\Lambda_{n+1}^{(0)}(\Lambda_{m+1}^{(0)})^{*}\frac{1}{8}[1+\cos(2\Omega t_3)e^{-2\Gamma\Omega^2 t_3}]$$

$$\times[A_{n+1,m+1}(t_2)-B_{n+1,m+1}(t_2)][1-\cos(2\Omega t_1)e^{-2\Gamma\Omega^2 t_1}]+\Lambda_{n+1}^{(0)}(\Lambda_{m}^{(0)})^{*}i\frac{e^{-i\varphi_3}}{8}\sin(2\Omega t_3)e^{-2\Gamma\Omega^2 t_3}$$

$$\times e^{i\varphi_2}[C_{n+1,m}(t_2)+D_{n+1,m}(t_2)][1-\cos(2\Omega t_1)e^{-2\Gamma\Omega^2 t_1}]-\Lambda_{n+1}^{(0)}(\Lambda_{m}^{(0)})^{*}\frac{i}{8}[1+\cos(2\Omega t_3)e^{-2\Gamma\Omega^2 t_3}]$$

$$\times e^{i\varphi_2}[C_{n+1,m+1}(t_2)+D_{n+1,m+1}(t_2)]e^{-i\varphi_1}\sin(2\Omega t_1)e^{-2\Gamma\Omega^2 t_1}-\Lambda_{n}^{(0)}(\Lambda_{m-1}^{(0)})^{*}\frac{i}{8}[1-\cos(2\Omega t_3)e^{-2\Gamma\Omega^2 t_3}]$$

$$\times e^{i\varphi_2}[C_{n,m}(t_2)-D_{n,m}(t_2)]e^{-i\varphi_1}\sin(2\Omega t_1)e^{-2\Gamma\Omega^2 t_1}(1-\delta_{m,0})-\Lambda_{n}^{(0)}(\Lambda_{m+1}^{(0)})^{*}i\frac{e^{i\varphi_3}}{8}\sin(2\Omega t_3)e^{-2\Gamma\Omega^2 t_3}$$

$$\times e^{-i\varphi_2}[-C_{n,m+1}(t_2)+D_{n,m+1}(t_2)][1-\cos(2\Omega t_1)e^{-2\Gamma\Omega^2 t_1}]+\Lambda_{n}^{(0)}(\Lambda_{m}^{(0)})^{*}\frac{1}{8}[1-\cos(2\Omega t_3)e^{-2\Gamma\Omega^2 t_3}]$$

$$\times[A_{n,m}(t_2)+B_{n,m}(t_2)][1-\cos(2\Omega t_1)e^{-2\Gamma\Omega^2 t_1}]-\Lambda_{n}^{(0)}(\Lambda_{m}^{(0)})^{*}\frac{e^{i\varphi_3}}{8}\sin(2\Omega t_3)e^{-2\Gamma\Omega^2 t_3}[A_{n,m+1}(t_2)$$

$$+B_{n,m+1}(t_2)]e^{-i\varphi_1}\sin(2\Omega t_1)e^{-2\Gamma\Omega^2 t_1}+\Lambda_{n}^{(0)}(\Lambda_{m-1}^{(0)})^{*}i\frac{e^{-i\varphi_3}}{8}\sin(2\Omega t_3)e^{-2\Gamma\Omega^2 t_3}e^{i\varphi_2}[C_{n+1,m}(t_2)$$

$$-D_{n+1,m}(t_2)][1+\cos(2\Omega t_1)e^{-2\Gamma\Omega^2 t_1}](1-\delta_{m,0})+\Lambda_{n}^{(0)}(\Lambda_{m+1}^{(0)})^{*}\frac{i}{8}[1+\cos(2\Omega t_3)e^{-2\Gamma\Omega^2 t_3}]$$

$$\times e^{-i\varphi_2}[-C_{n+1,m+1}(t_2)+D_{n+1,m+1}(t_2)]e^{i\varphi_1}\sin(2\Omega t_1)e^{-2\Gamma\Omega^2 t_1}-\Lambda_{n}^{(0)}(\Lambda_{m}^{(0)})^{*}\frac{e^{-i\varphi_3}}{8}\sin(2\Omega t_3)e^{-2\Gamma\Omega^2 t_3}$$

$$\times[A_{n+1,m}(t_2)+B_{n+1,m}(t_2)]e^{i\varphi_1}\sin(2\Omega t_1)e^{-2\Gamma\Omega^2 t_1}+\Lambda_{n}^{(0)}(\Lambda_{m}^{(0)})^{*}\frac{1}{8}[1+\cos(2\Omega t_3)e^{-2\Gamma\Omega^2 t_3}]$$

$$\times[A_{n+1,m+1}(t_2)+B_{n+1,m+1}(t_2)][1+\cos(2\Omega t_1)e^{-2\Gamma\Omega^2 t_1}],$$

where $\varphi_1$, $\varphi_2$, and $\varphi_3$ are the laser pulse phases for the first carrier, the Jaynes-Cummings, and the second carrier pulses, respectively. Note that, for $\Gamma=0$ we obtain from the above expressions the expected results without noise.

## APPENDIX C

In this appendix we show that a higher fidelity of the sculpted state, with regard to the desired state, does not implicate that the shape of the Wigner-distribution function of such sculpted state must be close to that of the desired state. We start by showing that for a desired state $|\Xi\rangle$ there is an infinite set of the sculpted states $|\Lambda_\lambda\rangle$ with the same fidelity $\mathcal{F}=|\langle\Lambda_\lambda|\Xi\rangle|^2$, the label $\lambda$ standing for a continuous real parameter or a set of continuous real parameters to be defined below. In order to simplify our discussion we consider a desired vibrational state in the two-dimensional Fock space $\{|0\rangle,|1\rangle\}$: $|\Xi\rangle=(|0\rangle+|1\rangle)/\sqrt{2}$. In this case, $\lambda$ reduces to a single continuous parameter since the set of states displaying the same fidelity $\mathcal{F}$ (represented by unit vectors in the so-called Bloch sphere of $\mathbb{R}^3$, in analogy with spin-1/2 states [41]), satisfy $|\Lambda_\lambda\rangle=e^{i\phi_0}(\lambda|0\rangle+e^{i(\phi_1-\phi_0)}\sqrt{1-\lambda^2}|1\rangle)$,

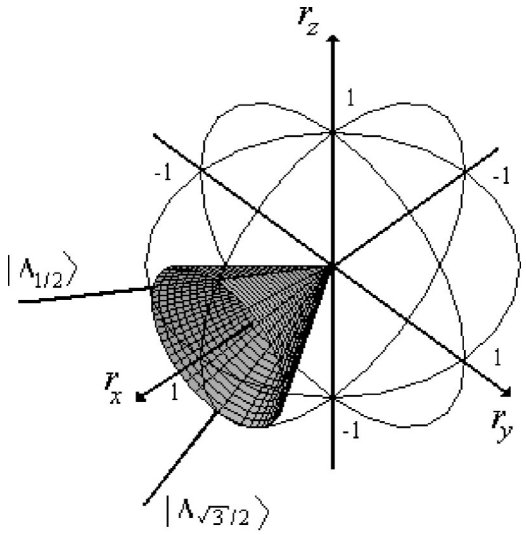


FIG. 5. The cone around the axis $r_x$ displayed in this figure, represents an infinite set of unit-vector states $|\Lambda_\lambda\rangle$ having the same fidelity $\mathcal{F}=(2+\sqrt{3})/4$ with respect to the state $|\Xi\rangle$. The circles around the figure represent the contours of the unit-Bloch sphere.

with

$$\phi=\phi_1-\phi_0=\arccos\frac{\mathcal{F}-1/2}{\lambda\sqrt{1-\lambda^2}}. \tag{C1}$$

The components $r_i=\mathrm{Tr}\,\sigma_i|\Lambda_\lambda\rangle\langle\Lambda_\lambda|$ of the states $|\Lambda_\lambda\rangle$ in the Bloch sphere, for $i=x,y,z$ and $\sigma_i$ referring to the Pauli pseudospin operators, read

$$\begin{aligned} r_x&=2\mathcal{F}-1,\\ r_y&=\pm 2[\lambda^2(\lambda^2-1)+(\mathcal{F}-1/2)^2],\\ r_z&=2\lambda^2-1, \end{aligned} \tag{C2}$$

where the signal $+$ $(-)$ in $r_y$ corresponds to positive (negative) values of $\phi$. Next, choosing $\mathcal{F}=(2+\sqrt{3})/4\approx 0.933$, it follows only two states with $\phi=0$ $(r_y=0)$: $|\Lambda_{1/2}\rangle=(|0\rangle+\sqrt{3}|1\rangle)/2$ and $|\Lambda_{\sqrt{3}/2}\rangle=(\sqrt{3}|0\rangle+|1\rangle)/2$, and an infinite set of states with $\phi\neq 0$. All these states, with Bloch vectors lying in the cone displayed in Fig. 5, present the same fidelity $\approx 0.933$, but different Wigner-distribution functions. Figures 6(a–c) display the Wigner functions for the states $|\Xi\rangle$, $|\Lambda_{1/2}\rangle$ and $|\Lambda_{\sqrt{3}/2}\rangle$, respectively, showing that although $|\Lambda_{1/2}\rangle$ and $|\Lambda_{\sqrt{3}/2}\rangle$ present the same fidelity with respect to $|\Xi\rangle$, Figs. 6(b,c) exhibit completely different shapes compared to Fig. 6(a). It is worth mention that the Wigner function varies continuously when $|\Lambda_\lambda\rangle$ evolves continuously from $|\Lambda_{1/2}\rangle$ to $|\Lambda_{\sqrt{3}/2}\rangle$ (going, in positive $z$ direction, through the bottom to the top of the cone in Fig. 5, in clockwise or counterclockwise direction depending on the signal of $r_y$).

The same analysis holds for the statistical mixtures

$$\begin{aligned} \rho_\lambda(\varkappa)=\lambda^2|0\rangle\langle 0|+(1-\lambda^2)|1\rangle\langle 1|+\varkappa\lambda\sqrt{1-\lambda^2}(e^{-i\phi}|0\rangle\langle 1\\ |+e^{i\phi}|1\rangle\langle 0|), \end{aligned} \tag{C3}$$

where the parameter $\varkappa\in[0,1]$ accounts for the purity of the density operator $\rho_\lambda(\varkappa)$, in a way that $\varkappa\neq 1$ imposes that Tr

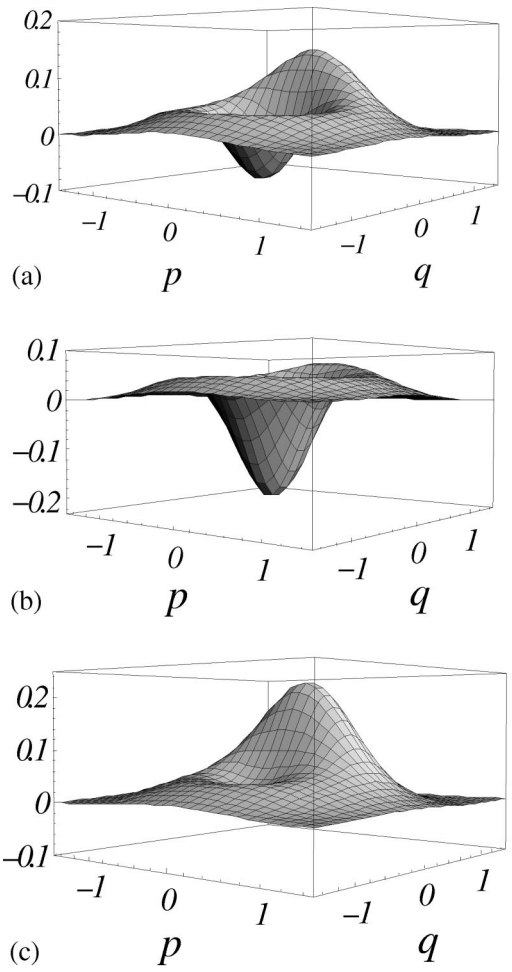


FIG. 6. Wigner-distribution functions for (a) the desired state $|\Xi\rangle$ and the two states lying in the cone of Fig. 5, with $\phi=0$: (b) $|\Lambda_{1/2}\rangle$ and (c) $|\Lambda_{\sqrt{3}/2}\rangle$.

$\{[\rho_\lambda(\varkappa)]^2\}<1$. For a given value of $\varkappa$, it follows an infinite set of statistical mixtures presenting the same fidelity $\mathcal{F}=\langle\Xi|\rho_\lambda(\varkappa)|\Xi\rangle$ when

$$\phi=\arccos\frac{\mathcal{F}-1/2}{\varkappa\lambda\sqrt{1-\lambda^2}}.$$

From a particular choice of $\varkappa=0.9$, $\mathcal{F}=0.8$, and $\lambda=0.7$, we obtain a statistical mixture displaying a Wigner-distribution

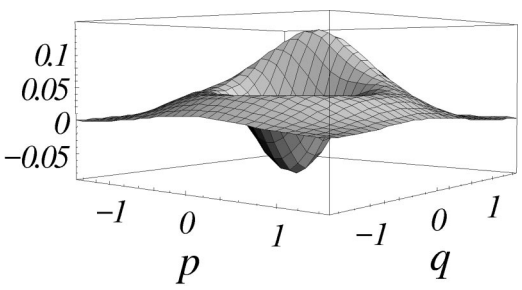


FIG. 7. Wigner-distribution function for the statistical mixture $\rho_\lambda(\varkappa)$ with a particular choice of $\varkappa=0.90$, $\mathcal{F}=0.85$, and $\lambda=0.70$.

function, depicted in Fig. 7, whose shape seems to be close to that in Fig. 6(a) than those in Figs. 6(b,c), although its fidelity is smaller than 0.933.

When considering the truncated-Fock space with more than two dimension, say $\{|0\rangle,|1\rangle,|2\rangle\}$, it follows a set of two real parameters for describing the set of states in a sphere of $\mathbb{R}^4$, and so on. Finally, we mention that our optimization protocol described in Sec. V is based on the maximization of the above-defined fidelity, the overlap between the sculpted and the desired state, which represents a particular measure of distance between vectors in Hilbert space, and cannot be inferred from the Wigner-distribution function.


[1] M. Brune, E. Hagley, J. Dreyer, X. Maitre, A. Maali, C. Wunderlich, J. M. Raimond, and S. Haroche, Phys. Rev. Lett. **77**, 4887 (1996).

[2] I. L. Chuang, L. M. K. Vandersypen, X. Zhou, D. W. Leung, and S. Lloyd, Nature (London) **393**, 143 (1998), and references therein.

[3] K. Vogel, V. M. Akulin, W. P. Schleich, Phys. Rev. Lett. **71**, 1816 (1993); M. H. Y. Moussa and B. Baseia, Phys. Lett. A **245**, 335 (1998).

[4] A. S. Parkins, P. Marte, P. Zoller, and H. J. Kimble, Phys. Rev. Lett. **71**, 3095 (1993).

[5] C. K. Law and J. H. Eberly, Phys. Rev. Lett. **76**, 1055 (1996).

[6] B. M. Garraway, B. Sherman, H. Moya-Cessa, P. L. Knight, and G. Kurizki, Phys. Rev. A **49**, 535 (1994).

[7] S. M. Barnett and D. T. Pegg, Phys. Rev. Lett. **76**, 4148 (1996).

[8] M. Dakna, J. Clausen, L. Knöll, and D.-G. Welsh, Phys. Rev. A **59**, 1658 (1999).

[9] R. L. de Matos Filho and W. Vogel, Phys. Rev. Lett. **76**, 608 (1996).

[10] B. Kneer and C. K. Law, Phys. Rev. A **55**, 2096 (1996).

[11] G. Brobný, B. Hladký, and V. Bužek, Phys. Rev. A **58**, 2481 (1998).

[12] E. Solano, R. L. de Matos Filho, and N. Zagury, Phys. Rev. A **59**, 2539 (1999).

[13] H. Moya-Cessa, S. Wallentowitz, and W. Vogel, Phys. Rev. A **59**, 2920 (1999).

[14] M. Brune, S. Haroche, J. M. Raimond, L. Davidovich, and N. Zagury, Phys. Rev. A **45**, 5193 (1992).

[15] D. M. Meekhof, C. Monroe, B. E. King, W. M. Itano, and D. J. Wineland, Phys. Rev. Lett. **76**, 1796 (1996).

[16] B. T. H. Varcoe, S. Brattke, M. Weidinger, and H. Walther, Nature (London) **403**, 743 (2000).

[17] C. Monroe, D. M. Meekhof, B. E. King, and D. J. Wineland, Science **272**, 1131 (1996).

[18] D. M. Meekhof, C. Monroe, B. E. King, W. M. Itano, and D. J. Wineland, Phys. Rev. Lett. **77**, 4281 (1996); W. M. Itano, C. Monroe, D. M. Meekhof, D. Leibfried, B. E. King, and D. J. Wineland, e-print quant-ph/9702038 (1997); D. Leibfried, D. M. Meekhof, C. Monroe, B. E. King, W. M. Itano, and D. J. Wineland, J. Mod. Opt. **44**, 2485 (1997); D. M. Meekhof, D. Leibfried, C. Monroe, B. E. King, W. M. Itano, and D. J. Wineland, Braz. J. Phys. **27**, 178 (1997).

[19] D. J. Wineland, J. J. Bollinger, W. M. Itano, and D. J. Heinzen, Phys. Rev. A **50**, 67 (1994); D. J. Wineland, J. J. Bollinger, W. M. Itano, F. L. Moore, and D. J. Heinzen *ibid.* **46**, R6 797 (1992).

[20] C. J. Myatt, B. E. King, Q. A. Turchette, C. A. Sackett, D. Kielpinski, W. M. Itano, C. Monroe, and D. J. Wineland, Nature (London) **403**, 269 (2000).

[21] J. F. Poyatos, J. I. Cirac, and P. Zoller, Phys. Rev. Lett. **77**, 4728 (1996).

[22] C. H. Roos, Th. Zeiger, H. Rohdle, H. C. Nägerl, J. Eschnner, D. Libfried, F. Schmidt-kaler, and R. Blatt, Phys. Rev. Lett. **83**, 4713 (1999).

[23] S. Schneider and G. H. Milburn, Phys. Rev. A **57**, 3748 (1998).

[24] S. Schneider and G. H. Milburn, Phys. Rev. A **59**, 3766 (1999).

[25] D. F. James, Phys. Rev. Lett. **81**, 3417 (1998).

[26] M. Murao and P. L. Knight, Phys. Rev. A **58**, 663 (1998).

[27] C. Di Fidio and W. Vogel, Phys. Rev. A **62**, 031802 (2000).

[28] D. J. Wineland, C. Monroe, W. M. Itano, L. Leibfried, B. E. King, and D. M. Meekhof, J. Res. Natl. Inst. Stand. Technol. **103**, 259 (1998).

[29] R. M. Serra, N. G. de Almeida, C. J. Villas-Bôas, and M. H. Y. Moussa, Phys. Rev. A **62**, 043810 (2000).

[30] N. G. de Almeida, R. Napolitano, and M. H. Y. Moussa, Phys. Rev. A **62**, 033815 (2000).

[31] N. G. de Almeida, P. B. Ramos, R. M. Serra, and M. H. Y. Moussa, J. Opt. B: Quantum Semiclass. Opt. **2**, 792 (2000).

[32] S. M. Barnett and D. T. Pegg, Phys. Rev. Lett. **76**, 4148 (1996).

[33] B. Baseia, M. H. Y. Moussa, and V. S. Bagnato, Phys. Lett. A **231**, 331 (1997).

[34] L. Davidovich, M. Orsag, N. Zagury, Phys. Rev. A **54**, 5113 (1996).

[35] J. Steinbach, J. Twanley, and P. L. Knight, Phys. Rev. A **56**, 4815 (1997); H. Zeng, Y. Wang, and Y. Segawa, *ibid.* **59**, 2174 (1999).

[36] M. A. Nielsen and I. L. Chuang,*Quantum Computation and Quantum Information* (Cambridge University Press, Cambridge, 2000); J. Preskill and A. Kitaev (unpublished) http://www.theory.caltech.edu/~preskill/ph229; R. P. Feynman, in *Feynman Lectures on Computation*, edited by A. J. G. Hey and R. W. Allen (Addison-Wesley, Reading, MA 1996).

[37] W. D. José and S. S. Mizrahi, J. Opt. B: Quantum Semiclassical Opt. **2**, 306 (2000).

[38] M. Freyberger, Phys. Rev. A **51**, 3347 (1995).

[39] J. Dalibard, Y. Castin, and K. Molmer, Phys. Rev. Lett. **68**, 580 (1992); R. Dum, P. Zoller, and H. Ritsch, Phys. Rev. A **45**, 4879 (1992).

[40] C. Monroe, D. M. Meekhof, B. E. King, W. M. Itano, and D. J. Wineland, Phys. Rev. Lett. **75**, 4714 (1995).

[41] R. P. Feynman, F. L. Vernon, and R. W. Hellwarth, J. Appl. Phys. **28**, 49 (1957).